RESEARCH ARTICLE

Key Points:
- The influence of eddies on surface chlorophyll concentrations varies regionally
- Eddy-induced chlorophyll anomalies are linked to four biophysical mechanisms
- This study provides a baseline to which models and in situ data can be compared

Correspondence to:
P. Gaube,
pgaube@whoi.edu

Regional variations in the influence of mesoscale eddies on near-surface chlorophyll

Peter Gaube[1], Dennis J. McGillicuddy Jr.[1], Dudley B. Chelton[2], Michael J. Behrenfeld[3], and Peter G. Strutton[4,5]

[1]Department of Applied Ocean Physics and Engineering, Woods Hole Oceanographic Institution, Woods Hole, Massachusetts, USA, [2]College of Earth, Ocean and Atmospheric Sciences, Oregon State University, Corvallis, Oregon, USA, [3]Department of Botany and Plant Pathology, Oregon State University, Corvallis, Oregon, USA, [4]Institute for Marine and Antarctic Studies, University of Tasmania, Hobart, Tasmania, Australia, [5]Australian Research Council Centre of Excellence for Climate System Science, University of Tasmania, Hobart, Tasmania, Australia

Abstract Eddies can influence biogeochemical cycles through a variety of mechanisms, including the excitation of vertical velocities and the horizontal advection of nutrients and ecosystems, both around the eddy periphery by rotational currents and by the trapping of fluid and subsequent transport by the eddy. In this study, we present an analysis of the influence of mesoscale ocean eddies on near-surface chlorophyll (CHL) estimated from satellite measurements of ocean color. The influences of horizontal advection, trapping, and upwelling/downwelling on CHL are analyzed in an eddy-centric frame of reference by collocating satellite observations to eddy interiors, as defined by their sea surface height signatures. The influence of mesoscale eddies on CHL varies regionally. In most boundary current regions, cyclonic eddies exhibit positive CHL anomalies and anticyclonic eddies contain negative CHL anomalies. In the interior of the South Indian Ocean, however, the opposite occurs. The various mechanisms by which eddies can influence phytoplankton communities are summarized and regions where the observed CHL response to eddies is consistent with one or more of the mechanisms are discussed. This study does not attempt to link the observed regional variability definitively to any particular mechanism but provides a global overview of how eddies influence CHL anomalies.

1. Introduction

Mesoscale eddies with spatial scales of $O(100\text{km})$ are ubiquitous features of the World Ocean, occupying ~25% of the ocean's surface area at any given time [*Chaigneau et al.*, 2009]. The mechanisms by which mesoscale ocean eddies influence marine phytoplankton can be segregated into three primary processes, namely, horizontal advection of phytoplankton, vertical flux of nutrients and phytoplankton, and eddy influence on stratification and hence on upper ocean mixing. More specifically, eddy surface currents can stir the ambient chlorophyll field by advecting phytoplankton around eddy peripheries [*Abraham*, 1998; *Siegel et al.*, 2007, 2011; *Chelton et al.*, 2011a]. Eddies can also trap parcels of water during formation, resulting in the advection of ecosystems, nutrients, and other water properties away from the region of eddy formation [*Pearce and Griffiths*, 1991; *Lehahn et al.*, 2011; *Early et al.*, 2011]. In contrast to horizontal advection, vertical fluxes of nutrients and phytoplankton can result from isopycnal displacement during eddy intensification [*Falkowski et al.*, 1991; *McGillicuddy et al.*, 1998], eddy decay [*Franks et al.*, 1986], and eddy-induced Ekman pumping resulting from eddy surface currents and sea surface temperature anomalies [*Martin and Richards*, 2001; *McGillicuddy et al.*, 2007; *Gaube*, 2012; *Gaube et al.*, 2013]. Eddies also influence stratification, potentially modulating light availability as a result of eddy effects on mixed layer depth [*Lévy et al.*, 1998, 1999; *Gaube et al.*, 2013].

Generally, isopycnals are domed upward in cyclonic eddies and displaced downward in anticyclones. There are exceptions to this general vertical structure. For example, some anticyclonic eddies contain an intrathermocline lens of water within their cores, resulting in shoaled isopycnals in the upper ocean and depressed isopycnals below the lens. These anticyclones are often referred to as mode-water type eddies. The depressed deep isopycnals in mode-water type eddies overshadow the upward displaced near-surface isopycnals in terms of geostrophic velocities, resulting in anticyclonic rotation and sea surface height

anomalies (SSH) that are of the same sign as those of regular anticyclones. These two types of anticyclones therefore cannot be differentiated from satellite observations of SSH alone and in this study we delineate eddies only by their sense of rotation, and not by their vertical structure.

The response of phytoplankton communities to mesoscale eddies on time scales of weeks to months can be observed globally by combining contemporaneous measurements made by satellite altimeters, spectrometers, and scatterometers. The analysis presented here discusses the observed regional variability of the response of phytoplankton to eddies, as inferred from satellite observations of SSH and near-surface chlorophyll concentration (CHL). The primary measure of eddy influence on phytoplankton used here is the cross correlation between SSH and CHL anomalies, which exhibits significant phenomenological variation (Figure 1a). We show that the observed regional relationships between SSH and CHL can be attributed to one or more classes of biophysical interactions. In cases where multiple mechanisms may be at work, we identify the ambiguities. This study thus provides an observational baseline upon which focused process studies can be based to diagnose in more detail the mechanisms responsible for the observed regional variability in the response of phytoplankton to mesoscale eddies.

It is important to note that the satellite data products used in this study do not resolve the submesoscale, which can have a dramatic impact on both the physics and biology of the upper ocean [*Lévy et al.*, 2012]. To some degree, this submesoscale variability may be averaged out in the analyses presented herein. However, we cannot discount the possibility that some of the mesoscale patterns that we observe are influenced by the rectified impact of submesoscale motions. Quantification of the relationships among these scales is a topic of active research and will greatly benefit from higher resolution satellite data sets (e.g., Surface Water Ocean Topography [SWOT]) [*Fu and Ferrari*, 2008], in situ process studies, and modeling.

This paper is organized as follows. In section 2.1, we describe the SSH observations used to identify and track mesoscale eddies. Section 2.2 provides an overview of the Ekman pumping velocities estimated from satellite scatterometer winds. Section 2.3 describes the CHL observations and how the signatures of mesoscale eddies are isolated from the large-scale, background CHL fields. In section 2.4, we provide an overview of how eddy-centric composites are constructed to determine the average spatial structure and temporal evolution of eddy-driven SSH and CHL anomalies. Four mechanisms by which eddies influence near-surface CHL are discussed in detail in section 3. An overview of the observed global variability of each of these mechanisms is presented in section 4, along with global composites of eddy CHL anomalies. Section 5 discusses regional variability of the influence of eddies on near-surface CHL from consideration of five study regions: the Gulf Stream, Brazil-Malvinas Confluence, East Australia Current, California Current System, and the interior South Indian Ocean. A summary and the conclusions of this study are presented in section 6.

2. Methods

2.1. Sea Surface Height and Eddy Identification

This investigation of mesoscale biological-physical interactions is based on eddies with lifetimes of 12 weeks and longer which have been identified and tracked based on their signatures in SSH [*Chelton et al.*, 2011b]. The SSH fields analyzed here span the time period October 1992 through December 2011 from Collecte Localis Satellites (CLS/AVISO) at 7 day intervals on a 1/4° latitude by 1/4° longitude grid. A total of 28,928 anticyclones and 30,857 cyclones with lifetimes longer than 12 weeks were identified globally in the 19 year data record considered here (the altimeter-tracked eddy data set used in this analysis is available online at http://cioss.coas.oregonstate.edu/eddies). The SSH fields used in this study are the Reference Series constructed by merging TOPEX/Poseidon, Jason-1, or Jason-2 measurements with ERS-1, ERS-2, or ENVISAT [*Ducet et al.*, 2000]. Only measurements from two of these six altimeters are combined at any given time. The wavelength resolution of the merged SSH fields is about 2° in latitude by 2° in longitude [*Chelton et al.*, 2011b]. As described in Appendix A3 of *Chelton et al.* [2011b], the eddy radius scale that corresponds to a wavelength of 2° can be determined by fitting a Gaussian SSH structure to the positive half of a cosine with 2° wavelength, yielding a radius scale of 0.4° which corresponds to 40 km at 30° latitude. Therefore, eddies with radii smaller than about 40 km have thus been filtered out in the SSH fields of the AVISO Reference Series.

As described in detail in Appendix B of *Chelton et al.* [2011b], mesoscale eddies were identified and tracked based on closed contours of SSH. The eddy amplitude at each weekly time step along its trajectory is defined as the difference between the SSH at the eddy SSH extremum and the SSH around the outermost
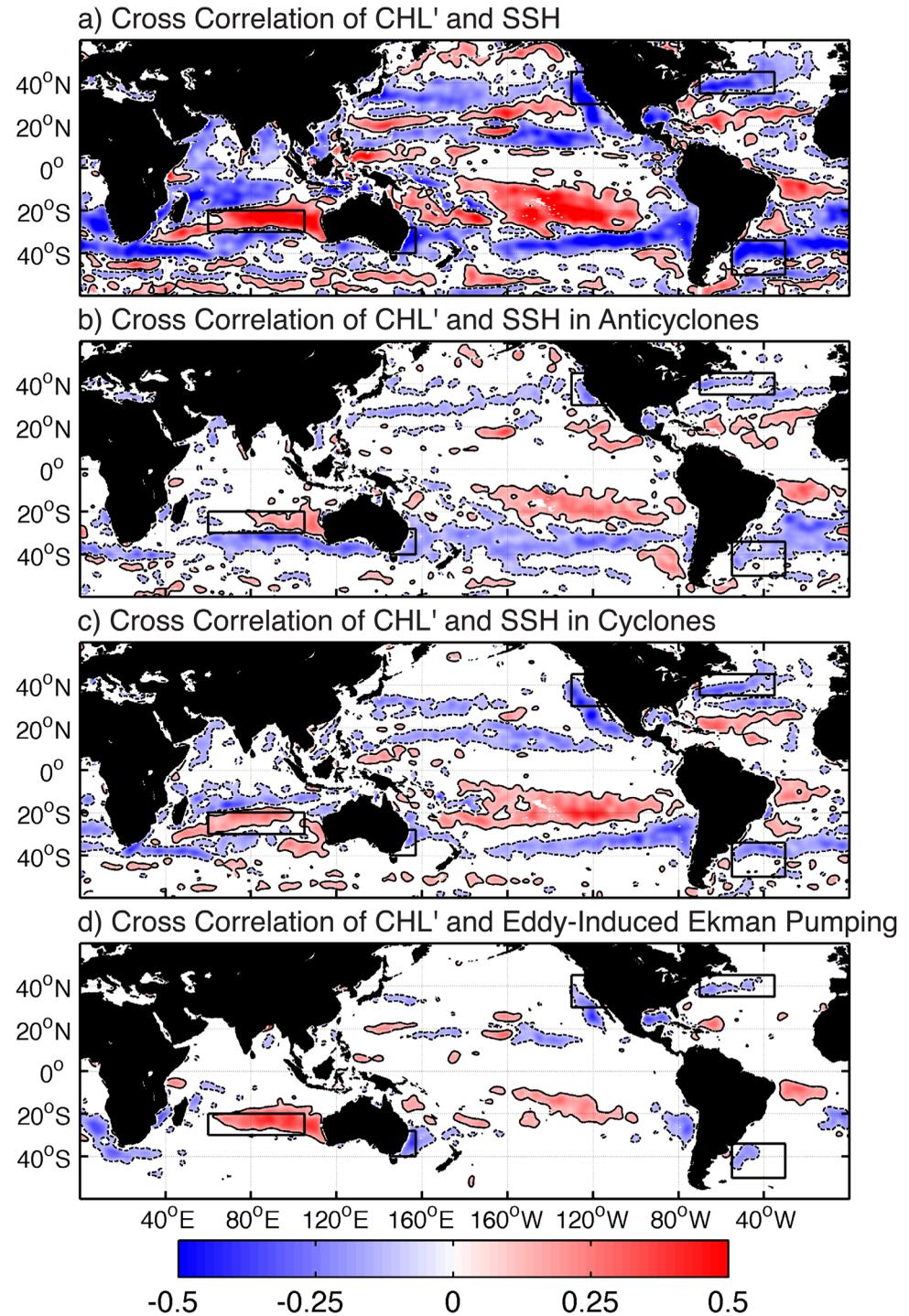
Figure 1. (a) Map of the cross correlation of CHL anomalies (CHL') and SSH at 0 time lag (r'_0). White areas correspond to correlations smaller than the estimated 95% significance level, calculated following the standard formula $\pm q_t(0.025, N^* - 2)/\sqrt{N^*}$ [*Von Storch and Zwiers*, 1999], where $q_t(0.025, N^* - 2)$ is the 2.5 percentage point of the Student's t distribution with $N^* - 2$ degrees of freedom. We esti-mate N^* as the number of weeks of data. Regions of significantly positive cross correlation ($r'_0 \geq 0.09$) are enclosed by a solid contour and regions of significantly negative cross correlation ($r'_0 \leq -0.09$) are enclosed by a dashed contour. (b) Map of the cross correlation of CHL' and SSH at 0 time lag only in the interiors of anticyclonic eddies with significant correlation regions contoured. (c) Same as Figure 1b, but for cross correlation in the interiors of cyclonic eddies. (d) Map of the cross correlation of CHL' and eddy-induced Ekman pumping at 0 time lag (r'_E). Regions of significantly positive cross correlation ($r'_E \geq 0.1$, for the ~10 year QuikSCAT data record) are enclosed by a solid contour and regions of significantly negative cross correlation ($r'_E \leq -0.1$) are enclosed by a dashed contour. The black boxes in all figures show the five study regions investigated in section 5. All maps were spatially smoothed with a half-power cutoff of 1° prior to plotting.

GAUBE ET AL.   3

closed contour of SSH. The eddy interior is defined to be the region inside this SSH contour. A minimum amplitude threshold of 1 cm must be met before a closed contour of SSH is defined as an eddy. The characteristic rotational speed of an eddy (U) is defined at each point along its trajectory as the average geostrophic speed along the SSH contour around which this quantity is maximum. The speed-based radius scale of the eddy, L_s, is defined to be the radius of a circle with area equal to that enclosed by the SSH contour associated with U.

In order to assess the nature of CHL anomalies entrained into eddies during their formation, the mean flow was juxtaposed with the mean CHL field (see section 2.3). For this purpose, we used the merged absolute dynamic topography fields distributed by CLS/AVISO [see *Rio et al.*, 2011, for details].

2.2. Ekman Pumping

Ekman pumping velocities were estimated from 10 m wind inferred from measurements by the SeaWinds scatterometer onboard the QuikSCAT satellite. The QuikSCAT mission began on 19 July 1999 and ended on 23 November 2009. Scatterometers infer equivalent neutral vector wind at 10 m relative to the moving sea surface [referred to as the relative wind, e.g., *Ross et al.*, 1985; *Chelton and Freilich*, 2005]. The relative wind estimated from QuikSCAT observations included both the influence of ocean surface currents on the equivalent neutral wind, as well as the effects of air-sea interaction occurring in *SST* frontal regions (see the reviews by *Small et al.* [2008] and *Chelton and Xie* [2010]). The relative equivalent neutral wind was converted to surface stress (τ) using the neutral drag coefficient based on the formulation used in the Coupled Ocean-Atmosphere Response Experiment, version 3.0 (COARE 3.0) bulk flux algorithm [*Fairall et al.*, 2003].

The curl of the surface stress $\nabla \times \tau$ was calculated in-swath for each orbit and gridded onto a $1/4° \times 1/4°$ grid using a low-pass filter with a half-power cutoff of 80 km. Ekman pumping was computed as

$$W_E = \frac{\nabla \times \tau}{\rho_o f},$$
(1)

where $\rho_o = 1020$ kg m^{-3} is the (assumed constant) surface density of sea water and $f = 2\Omega \cos \theta$ is the Coriolis parameter for latitude θ and Earth rotation rate Ω. In this study, we consider only the contribution to the total Ekman pumping that results from the curl of the surface stress (equation (1)), sometimes referred to as "linear Ekman pumping." We neglect the vorticity gradient contribution to total Ekman pumping, sometimes referred to as "nonlinear Ekman pumping," which results from the interaction of the surface stress with gradients in the surface current vorticity [e.g., *Thomas and Rhines*, 2002; *Thomas*, 2005; *Mahadevan et al.*, 2008; *Gaube et al.*, 2014]. Although the latter can result in higher vertical velocities than the linear Ekman pumping, vorticity gradient-induced vertical motions tend to average to approximately zero along rotational streamlines in eddy interiors [*McGillicuddy et al.*, 2008]. Moreover, because the locations of the upwelling/downwelling cells associated with the nonlinear terms depend on the direction of the wind, they do not persist geographically as long as those driven by equation (1) and, as such, do not afford as much time for a biological response to accumulate. Last, the $1/4°$ grid resolution of the altimetric SSH analysis from which geostrophic surface currents are computed is likely not sufficient to represent the most energetic nonlinear Ekman pumping, which takes place at the submesoscale [*Mahadevan et al.*, 2008].

Because the wind field has scales larger than the $O(100$ km$)$ scales of midlatitude mesoscale eddies, the curl of the surface stress is mostly attributable to the vorticity of the eddy surface currents. To be consistent with the $\sim$35 day *e*-folding time scale of the covariance function of the objective analysis procedure used by AVISO to produce the SSH fields [*Ducet et al.*, 2000; *Chelton et al.*, 2011b], the W_E fields considered in this study were constructed at the same 7 day intervals as the SSH observations with temporal low-pass filtering with a half-power filter cutoff of 30 days. The W_E fields were then spatially high-pass filtered with half-power filter cutoffs of 6° of longitude by 6° latitude to remove large-scale features unrelated to the mesoscale variability that is of interest in this study. These smoothing parameters were chosen as a compromise between attenuating unwanted large-scale variability in the W_E fields while retaining variability associated with mesoscale eddies.

2.3. Near-Surface Chlorophyll Concentration

Observations of near-surface CHL were obtained from the Sea-viewing Wide Field-of-view Sensor (SeaWiFS) onboard the Orbview-2 satellite, also known as SeaStar. The 13 year SeaWiFS mission began on 19 September 1997 and ended on 10 September 2010. The Garver-Siegel-Maritorena (GSM) semianalytical ocean color

algorithm [*Garver and Siegel*, 1997; *Maritorena et al.*, 2002; *Siegel et al.*, 2002] was used to estimate CHL from ocean color measurements made by SeaWiFS.

Estimates of chlorophyll concentration made from satellite observations of ocean color are limited to the near-surface. Throughout much of the world ocean, however, the largest chlorophyll concentrations are found near the base of the euphotic zone. The relationship between CHL and vertically integrated chlorophyll concentration also depends on abiotic factors such as water clarity (the depth of the euphotic zone) and stratification (the depth of the surface mixed layer). In some regions, therefore, CHL does not provide a reliable estimate of the vertically integrated chlorophyll concentration.

It is important to note, however, that in most environments, primary productivity declines exponentially with depth and the contribution of deep chlorophyll maxima to water column integrated productivity is small. For a global overview, see Figure 1 in *Behrenfeld and Falkowski* [1997] which generally shows an exponential decrease in productivity with depth, with the peak of productivity in the first optical depth, defined as the inverse of the light extension coefficient at 490 nm (Kd490).

Satellite-derived CHL is indicative of variability in the biomass of primary producers. The relationship between phytoplankton biomass and chlorophyll can become tenuous when investigating anomalies of the CHL field. This is because CHL varies not only as a function of biomass but also as a result of physiological acclimation to light availability (photoacclimation), temperature, nutrient limitation, as well as phytoplankton community composition [*Laws and Bannister*, 1980; *Cullen*, 1982; *Geider*, 1987; *Falkowski and LaRoche*, 1991; *Behrenfeld et al.*, 2005, 2008]. However, analysis of near-surface phytoplankton biomass, CHL, and mixed layer light levels estimated from satellite observations and Argo float profiles concluded that in the regions considered in section 5, eddy-induced variations in CHL result primarily from changes in biomass and not photoacclimation [*Gaube*, 2012; *Gaube et al.*, 2013]. Therefore, this investigation of CHL variability in eddies can provide valuable insight into the influence of eddies on phytoplankton biomass and ultimately on primary production. This is particularly important given the ubiquity and abundance of eddies throughout most of the World Ocean.

Since clouds are opaque in the visible spectrum, CHL estimates can be made only in cloud-free conditions. Data gaps during cloudy conditions must be taken into consideration when filtering the ocean color data in order to obtain reasonable estimates of CHL in eddies. The CHL fields were first $\log_{10}$ transformed and averaged onto the same 1/4° latitude by 1/4° longitude grid as the SSH observations described in section 2.1. The log transformation accounts for the highly skewed distributions of the untransformed data that can occur in many regions of the World Ocean, especially in near-coastal regions [*Campbell*, 1995]. The time series of daily CHL values at each grid point were then low-pass loess filtered and gridded at weekly intervals to attenuate variability with periods shorter than 30 days and reduce data gaps from cloud contamination. The gridded $\log_{10}CHL$ fields were then transformed back to linear concentrations.

To isolate mesoscale spatial variability, the weekly maps of CHL were spatially high-pass filtered with the same half-power filter cutoffs of 6° in longitude by 6° in latitude applied to the W_E fields (section 2.2). The CHL anomaly fields (CHL') are defined as

$$CHL' = CHL - <CHL>, \tag{2}$$

where the $<>$ denotes the smoothed fields that are removed from the total fields to create the anomalies that are denoted with primes. To minimize filter edge effects caused by the exponential decay of ambient CHL away from the coast, observations within a radial span of 6 grid points (approximately 150 km) from any location identified as land were removed.

It is important to note that the log transformation was only applied to the CHL data to construct the 30 day smoothed maps. The analysis is performed on the non-log-transformed fields. The effect of log transformation of data in the eddy-centric coordinate system used here has been analyzed by *Gaube et al.* [2013; see their Appendix A], where it is shown that the eddy-centric composite averages are qualitatively similar when constructed from anomalies of either log-transformed or non-log-transformed data.

Fields of CHL' are suitable for computing direct correlations with SSH (section 3.5), but compositing multiple observations into eddy-centric coordinates (section 2.4) poses an additional challenge. Specifically, the magnitude of the eddy-driven CHL anomalies varies both geographically and seasonally. To help mitigate these

effects on eddy-centric composites, we normalized the anomalies at longitude x and latitude y by the long-term averaged background fields at the same location,

$$CHL''(x,y) = \frac{CHL'(x,y)}{\overline{CHL}(x,y)} \qquad (3)$$

where $\overline{CHL}(x,y)$ is the time-averaged background CHL field over the 13 year SeaWiFS data record. This simple normalization allows easy conversion of normalized anomalies back into concentrations.

To estimate the CHL content of eddies formed from lateral meanders of large-scale currents, we compute the cross-current CHL gradient, which is the CHL gradient calculated in a natural coordinate system. The two-dimensional natural, or stream-following coordinate system, is defined by an orthogonal pair of unit vectors that are oriented parallel and normal to the flow field at each point. Of interest to this study is only the local cross-current unit vector n, which is defined to be normal (orthogonal) to the surface current at each point. The component of the CHL gradient in the direction of n (the cross-current CHL gradient, $\partial CHL/\partial n$) provides insight into the relative alignment of the ambient CHL gradient perpendicular to the ocean surface current. The local cross-current coordinate n is defined here to be positive to the left of the current direction looking downstream. As such, regions of positive cross-current CHL gradient ($\partial CHL/\partial n > 0$) are characterized by higher CHL to the left of the current. Conversely, regions of negative cross-current CHL gradient ($\partial CHL/\partial n < 0$) are characterized by elevated CHL to the right of the current direction. As our interest here is to identify regions where, on average, eddies entrain elevated or suppressed CHL during formation, we computed the background, time-averaged cross-current CHL gradient, $\partial \overline{CHL}/\partial n$ from the meridional and zonal gradients of the 13 year averaged CHL field ($\overline{CHL}$) as

$$\frac{\partial \overline{CHL}}{\partial n} = -\sin\phi \, \frac{\partial \overline{CHL}}{\partial x} + \cos\phi \, \frac{\partial \overline{CHL}}{\partial y}, \qquad (4)$$

where ϕ is the direction of the geostrophic current estimated from the merged absolute dynamic topography and averaged over the 13 year SeaWiFS data record (see section 2.1). As a result of the order-of-magnitude decrease of CHL away from the coast in the boundary current systems considered here, the time-averaged cross-current $\overline{CHL}$ gradient also is larger in magnitude close to the coast. As the focus of this study is the influence of eddies on CHL in the open ocean, $\partial \overline{CHL}/\partial n$ was normalized by the local mean chlorophyll $\overline{CHL}$, to allow open ocean regions to be compared to coastal regions.

2.4. Collocation of Satellite Observations to the Interiors of Mesoscale Eddies

To evaluate the CHL response to mesoscale eddies, satellite-based estimates of CHL'' described in section 2.3 were collocated to the interior of each eddy realization identified from the altimeter data (section 2.1) for the 9 year period January 2001 through November 2009, during which concurrent measurements of ocean color, SSH, and Ekman pumping are available. The collocated values were referenced geographically to the eddy SSH extremum and interpolated onto a high-resolution grid with radial distance from the eddy center normalized by the eddy radius scale L_s. This normalization allows composites to be constructed from thousands of weekly eddy observations on a common grid defined by the horizontal size of each individual eddy.

As will become apparent in the global composite averages presented in section 4.4 and has been previously shown by *Chelton et al.* [2011a] from composite averages of midlatitude eddies, eddy surface currents influence CHL predominantly by horizontal advection of the background CHL field by the azimuthal velocity within the eddy interior. As in *Chelton et al.* [2011a] and *Gaube et al.* [2013], global composites of mesoscale CHL'' were computed in a translating and rotated frame of reference determined by the orientation of the background CHL gradient, which was defined based on the $6° \times 6°$ smoothed CHL fields ($<CHL>$, equation (2)). When this ambient $<CHL>$ gradient vector had a nonzero northward or southward component, the eddy-centric CHL'' values were rotated to orient the background $<CHL>$ gradient vector at a polar angle of $90°$ or $-90°$, respectively.

The temporal evolution of CHL'' in eddies is used in section 5 to help distinguish between different mechanisms that influence the chlorophyll response. Time series of CHL'' are constructed as a function of eddy age by averaging weekly horizontally normalized CHL'' observations within a radial distance of L_s of the eddy SSH extremum. In section 5, we also show that the statistical significance of the composite averages

of CHL'' varies spatially. Observations located at grid locations where the composite averages are not significantly different from zero are excluded from the CHL'' time series.

3. Mechanisms By Which Eddies Influence Near-Surface CHL

The influence of eddies on near-surface CHL can be segregated into processes that advect nutrients and plankton, either horizontally or vertically, and those that modulate stratification. It has been argued that mesoscale variations in stratification primarily influence phytoplankton in regions where primary production is limited by light, rather than nutrients [*Lévy et al.*, 1998, 1999]. To assess whether the influence of mesoscale eddies on stratification significantly affects the results presented here, we repeated the analysis presented in section 5 after excluding observations during the winter, defined as the 3 month period when mixed layer depths were at a maximum, which is the time period during which the local photoautotrophic communities are likely light limited. The resultant composite averages and time evolution of CHL'' in eddies in the boundary current regions investigated here (the Gulf Stream, Brazil-Malvinas Confluence, East Australia Current, and California Current System) were nearly identical to those constructed from the year-round data sets. In the open ocean region considered in section 5, the interior South Indian Ocean, seasonal changes in the spatial structure of the composite averages and time evolution of CHL'' were observed. These seasonal changes are described in section 5 and were investigated in detail by *Gaube et al.* [2013]. As a result of the limited impact of seasonal variability in near-surface stratification on the CHL'' signatures of eddies in the boundary current regions considered here, we limit the examination of seasonal changes in the CHL'' response to eddies of the interior South Indian Ocean.

The horizontal advection of nutrients and plankton can be broken down into two mechanisms: eddy stirring, which occurs primarily around the peripheries of eddies, and the trapping and subsequent transport in the interiors of eddies. Likewise, upwelling and downwelling in eddies can also be segregated into vertical velocities resulting from the displacement of isopycnals during eddy intensification, and those generated by eddy-induced Ekman pumping as a result of the interactions of the ambient wind field with eddy-induced surface currents and sea surface temperature (SST) anomalies. These mechanisms are summarized in sections 3.1–3.4. Their manifestations in the covariability of SSH and CHL are described in section 3.5 and summarized in Table 1. We emphasize here that the CHL'' responses portrayed in sections 3.1–3.4 are for highly idealized scenarios in which only a single eddy-driven mechanism is active, with all other factors assumed to be unchanging. Specifically, we neglect any ecological variability (e.g., top-down control from grazing) that could modulate the CHL'' response to each of the individual mechanisms.

3.1. Eddy Stirring

The azimuthal advection of CHL around eddy peripheries is referred to here as eddy stirring. It has been shown to be the dominant mechanism, in a globally averaged sense, by which eddies influence CHL in the midlatitudes on time scales on the order of weeks to months and spatial scales larger than ∼2° [*Chelton et al.*, 2011a]. Eddy stirring occurs primarily along the peripheries of eddies.

For a westward propagating eddy, the leading edge advects the ambient CHL field poleward in anticyclones and equatorward in cyclones, and the opposite occurs at the trailing edge of the eddy. Consider, for example, a clockwise-rotating eddy (northern hemisphere anticyclone) in a northward $\overline{CHL}$ gradient, shown schematically in the top of Figure 2a. The western, leading edge of the eddy contains a negative CHL'' in the northwest quadrant and the eastern, trailing edge a positive CHL'' in the southeast quadrant. In the same background field, a counterclockwise-rotating eddy (northern hemisphere cyclone) will result in a positive anomaly in the southwest quadrant and a negative anomaly in the northeast quadrant (Figure 2a, bottom).

The sign and alignment of the dipole of CHL'' associated with eddy stirring are a function of the rotational sense of the eddy in relation to the direction of the ambient CHL field. The magnitudes of the leading and trailing poles of CHL'' are asymmetric, with the leading pole larger in magnitude. This asymmetry is presumably a result of the trailing edge of the eddy interacting with an ambient CHL field that has recently felt the influence of the leading edge of the eddy [*Chelton et al.*, 2011a]. The same asymmetric dipole is observed for eddy stirring of an ambient passive tracer field in a model simulation of quasigeostrophic eddies [*Chelton et al.*, 2011a].

Table 1. The Expected Sign of the Cross Correlation Between CHL' and SSH at Either Zero or Plus 4 Weeks Time Lag as a Result of the Four Mechanisms by Which Eddies Influence CHL Examined in This Study[a]

| | | Mechanism | | | |
| | | Stirring | Trapping | Intensification | Eddy-Ekman |
Eddy Type	CHL Gradient	+4 Week Time Lag	0 Time Lag	0 Time Lag	0 Tim Lag
N.H. cyclones	$\partial <CHL>/\partial y > 0$	−			
N.H. anticyclones	$\partial <CHL>/\partial y > 0$	−			
N.H. cyclones	$\partial <CHL>/\partial y < 0$	+			
N.H. anticyclones	$\partial <CHL>/\partial y < 0$	+			
S.H. cyclones	$\partial <CHL>/\partial y > 0$	+			
S.H. anticyclones	$\partial <CHL>/\partial y > 0$	+			
S.H. cyclones	$\partial <CHL>/\partial y < 0$	−			
S.H. anticyclones	$\partial <CHL>/\partial y < 0$	−			
N.H. cyclones or anticyclones	$\partial \overline{CHL}/\partial n < 0$		+		
S.H. cyclones or anticyclones	$\partial \overline{CHL}/\partial n > 0$		+		
N.H. cyclones or anticyclones	$\partial \overline{CHL}/\partial n > 0$		−		
S.H. cyclones or anticyclones	$\partial \overline{CHL}/\partial n < 0$		−		
N.H. or S.H. cyclones				−	+
N.H. or S.H. anticyclones				−	+

[a]The response of CHL to eddies is segregated by the sign of either the meridional ambient $<CHL>$ gradient ($\partial <CHL>/\partial y$) or the cross-current $\overline{CHL}$ gradient ($\partial \overline{CHL}/\partial n$). Eddies are either segregated by hemisphere (N.H. and S.H. are northern and southern hemisphere, respectively) or polarity.

We note that the upward displaced shallow isopycnals in mode-water type anticyclones act to reduce near-surface geostrophic velocities, which are dominated by the downward displaced isopycnals in the main thermocline. Observations in the Sargasso Sea, however, revealed that mode-water type anticyclones are readily detected in maps of SSH [*Sweeney et al.*, 2003; *McGillicuddy et al.*, 2007] and they have rotational velocities that are comparable to standard anticyclones. The CHL response to eddy stirring is therefore expected to be the very similar in regular anticyclones and mode-water type anticyclones.

Mechanisms by Which Mesoscale Eddies Influence Phytoplankton
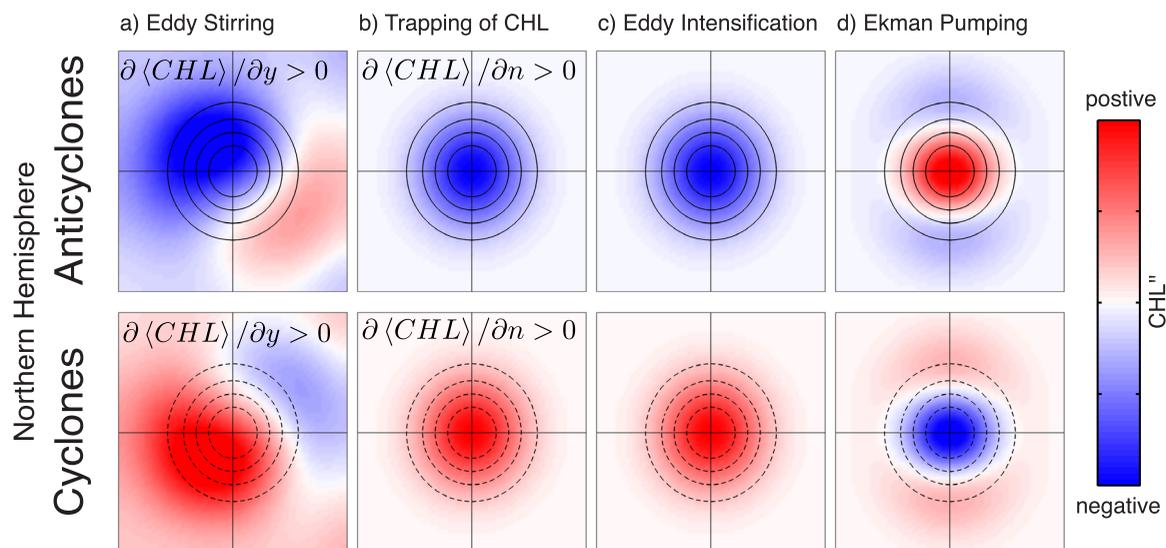### Spatial Structure

Figure 2. Schematic representations of the expected spatial structure of CHL'' overlaid with contours of SSH (negative SSH shown as dashed curves) associated with the four mechanisms investigated here by which eddies influence phytoplankton communities. (a) The azimuthal advection of phytoplankton communities around the peripheries of eddies (eddy stirring) for northern hemisphere eddies in a northward gradient of ambient CHL. (b) The trapping of the ambient CHL and nutrient field during the formation of northern hemisphere eddies in a region of positive cross-current background $\overline{CHL}$ gradient. (c) CHL response to vertical flux generated during eddy intensification. The $O(1 \, \text{m} \, \text{d}^{-1})$ upwelling and downwelling results in elevated and suppressed CHL in cyclones and anticyclones, respectively. (d) Eddy-induced Ekman pumping. The $O(10 \, \text{cm} \, \text{d}^{-1})$ downwelling and upwelling generates reduced CHL in cyclones and enhanced CHL in anticyclones, respectively.
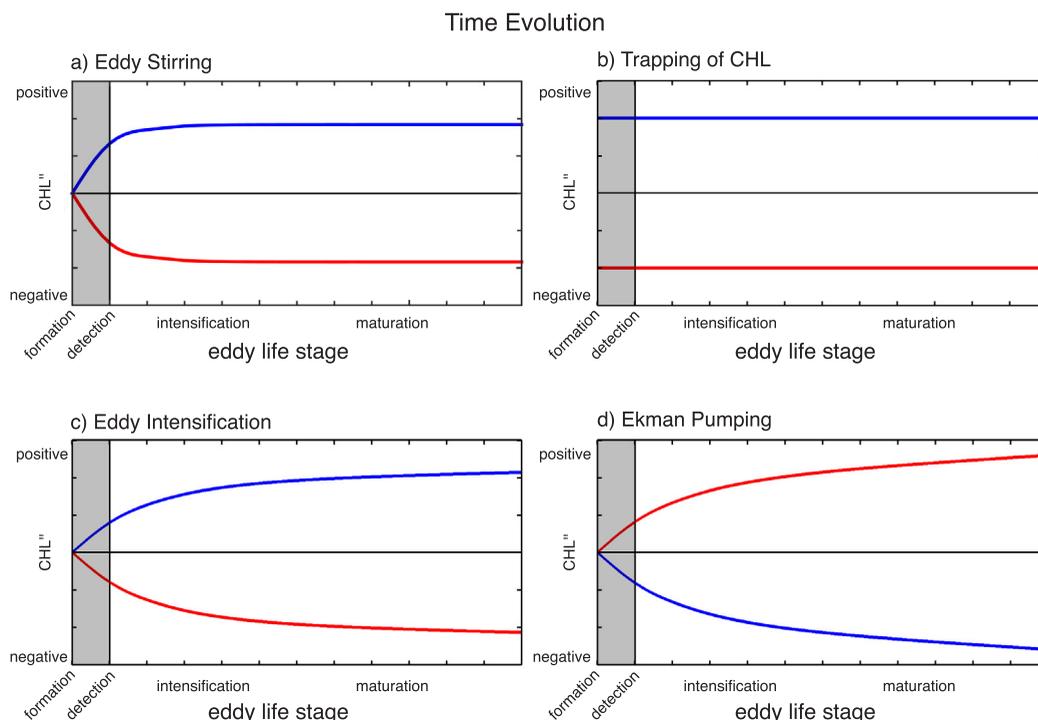
Figure 3. Schematic representations of the *CHL″* time series expected as a result of the four mechanisms by which eddies influence CHL investigated here, with anticyclones (clockwise rotation in the northern hemisphere) shown in red and cyclones (counterclockwise rotation in the northern hemisphere) in blue. The schematic time series are shown as a function of eddy life stage. (a) The azimuthal advection of phytoplankton communities around the peripheries of eddies (eddy stirring) for northern hemisphere eddies in a northward gradient of ambient CHL. (b) The trapping of the ambient CHL and nutrient field during the formation of northern hemisphere eddies in a region of positive cross-current background $\overline{CHL}$ gradient. (c) CHL response to vertical flux generated during eddy intensification. (d) CHL response to vertical flux generated by eddy-induced Ekman pumping. The beginning of the time series are shaded to indicate ambiguity in the expected *CHL″* in eddies from the time of eddy formation (week 0) until it is first detected by the automated eddy tracking procedure (week 1).

In addition to the expected spatial structure resulting from eddy stirring, we can also predict the expected *CHL″* time evolution. Because of the asymmetry of the dipoles, the total *CHL″* would be negative in anticyclones and positive in cyclones (Figure 3a) in the northern hemisphere eddies propagating in a northward ambient $<CHL>$ gradient considered above. The magnitude of the *CHL″* time series could change as a function of (1) rotational velocity, (2) the direction of the ambient $<CHL>$ gradient, (3) the eddy propagation speed, and (4) temporal variability from the growth and loss of the phytoplankton community. In the idealized schematic time series in Figure 3a, the latter three factors are assumed to be invariant, and the initial increase in stirring-induced *CHL″* reflects eddy spin-up (see section 3.3).

We note that submesoscale fronts can develop on the periphery of an eddy, generating upwelling and downwelling cells in elongated density fronts with vertical velocities on the order of 10 m d^{-1} [*Legal et al.*, 2007]. These submesoscale fronts are located in regions where water masses of different densities are forced to converge by the mesoscale flow field [*Lévy et al.*, 2012]. The upwelling and downwelling cells associated with these fronts are, however, not expected to be systematically oriented relative to the ambient CHL gradient—and as such they would tend to be smoothed out in composite averages of thousands of eddies. We therefore expect that the dipole pattern presented in Figure 2a is primarily a result of mesoscale rather than submesoscale processes.

3.2. Trapping of Ecosystems by Eddies
Nonlinear eddies, for which the rotational velocities of the eddy are faster than the eddy propagation speed, can trap fluid in their interiors [*McWilliams and Flierl*, 1979; *Flierl*, 1981]. Ecosystems trapped in eddies

during formation "prime" the eddy interior toward either elevated or suppressed phytoplankton concentration, depending on the ambient biological field in the region of formation. As nearly all extratropical eddies are observed to be nonlinear [*Chelton et al.*, 2011b], nutrients and phytoplankton are trapped in eddies as they propagate away from their region of origin. This trapping of fluid is eloquently shown in a recent idealized modeling study of the transport of a passive tracer by a monopole eddy [*Early et al.*, 2011].

The trapping of ecosystems has been observed in eddies formed from the pinching-off of meanders of the Gulf Stream. Early observations revealed that ecosystems in newly formed cyclonic Gulf Stream eddies (or rings) possessed elevated phytoplankton biomass at the base of the euphotic zone [*Backus et al.*, 1981], which decayed soon after eddy formation [*Wiebe et al.*, 1976]. The preferential entrainment of water with elevated phytoplankton and nutrient concentrations into either cyclonic or anticyclonic eddies is determined by the direction of the meandering current from which the eddies form and the direction of the ambient gradient in phytoplankton and nutrient concentration.

Cyclonic meanders entrain water from the shoreward side of the current during formation in poleward-flowing western boundary currents, such as the Gulf Stream, Kuroshio Current, and Brazil Current, and in equatorward-flowing eastern boundary currents such as the California Current, Peru-Chile Current, and Benguela Current. This water is generally higher in phytoplankton and nutrient concentration than the water seaward of the current, resulting in positive $\partial \overline{CHL}/\partial n$ as defined in section 2.3. These cyclonic meanders subsequently pinch off and form eddies that trap water with elevated nutrients and phytoplankton biomass in their interiors (Figure 2b, bottom). Conversely, anticyclonic meanders formed in the aforementioned boundary current systems entrain water from offshore, pinching off into anticyclonic eddies that trap water generally lower in phytoplankton concentration than the water closer to the coast (Figure 2b, top).

Undulating meanders of open ocean currents can also generate eddies that entrain the ambient phytoplankton concentration and the nutrients assimilated within these organisms. A case study example of the preferential entrainment of locally elevated CHL into the interiors of anticyclones formed in the South Indian Ocean was shown in Appendix B of *Gaube et al.* [2013], where a westward propagating anticyclonic meander of an eastward open ocean current was observed to advect elevated CHL from north to south along its western edge. Eventually, the meander pinched off to form an isolated anticyclonic mesoscale eddy with positive CHL'' trapped in its interior.

Assessing the source waters for mode-water anticyclones is more difficult because their formation can involve subduction of mode waters [*Ebbesmeyer and Lindstrom*, 1986], thus decoupling (at least temporarily) the near-surface and main-thermocline strata. As such, the source water in the euphotic zone of mode-water type anticyclones may not be predictable by $\partial \overline{CHL}/\partial n$.

The expected temporal evolution of CHL'' in trapped ecosystems, assuming all other factors remain constant, is a step function that takes place at the time of eddy formation. For the combination of current direction and background CHL gradient representative of most boundary current systems, as was considered schematically in Figure 2b, negative CHL'' would persist in anticyclones and positive CHL'' would persist in cyclones (Figure 3b). Following the trapping of fluid during eddy formation, exchange with the surrounding environment occurs [*Olson*, 1986; *d'Ovidio et al.*, 2013]. This exchange between the eddy interior and its surroundings would result in the decay of the CHL anomalies.

Additional biological and physical processes that could occur in the trapped interiors of these eddies have been omitted from the idealized temporal evolution shown in Figure 2b. For example, nutrients trapped in eddies during formation could be rapidly consumed by the phytoplankton communities, resulting in nutrient limitation and decreasing CHL. Alternatively, grazers initially present in the trapped fluid may vacate the eddy as environmental conditions change [*Wiebe and Flierl*, 1983] thereby affecting top-down controls on CHL. Such effects on the CHL anomalies associated with eddy trapping have not been included in the idealized time series shown in Figure 2b.

Note that the schematic examples shown in Figures 2b and 3b represent just one of several possible configurations, as described in section 3.5.

3.3. Upwelling and Downwelling During Eddy Intensification

Upwelling and downwelling generated during the intensification of eddies, often referred to as "eddy pumping" [*Falkowski et al.*, 1991], results in enhanced CHL in cyclones and depressed CHL in anticyclones

[*McGillicuddy et al.*, 1998; *Siegel et al.*, 1999, 2007, 2011]. Upwelling during the intensification of cyclones can enhance phytoplankton growth rates, resulting in elevated phytoplankton biomass and CHL (Figure 2c, bottom). The increase of nutrients in the cores of cyclones has been observed in the lee of the Hawaiian Islands [*Falkowski et al.*, 1991; *Benitez-Nelson et al.*, 2007] and in mid-ocean eddies in the Sargasso Sea [*McGillicuddy et al.*, 1998]. In contrast to the upwelling in cyclones, downwelling in anticyclones during intensification can result in negative anomalies of photoautotrophic biomass and growth rate from the downward transport of nutrients and phytoplankton to depths below the euphotic zone (Figure 2c, top).

The issue of intensification in mode-water type anticyclones is more complex because of their vertical structure. If the upward displaced shallow isopycnals are shoaled during eddy intensification, CHL is expected to increase and generate positive CHL''. If the deep isopycnals are depressed during eddy intensification, a near-surface CHL response would not be expected.

To estimate an order-of-magnitude scaling for the vertical velocities generated during eddy intensification, we use published observations of isopycnal displacements in eddies and the time it takes eddies to grow and reach a quasi-steady state. Measurements made at the Bermuda Atlantic Time series Study (BATS) mooring document isopycnal displacements of ≈50 m at the base of the euphotic zone during the passage of a cyclonic mid-ocean eddy [*Siegel et al.*, 1999]. To estimate the growth rate in eddy amplitude from our altimetric SSH observations, we used finite differences of the eddy amplitude time series computed from the median amplitude of hundreds of individual eddy observations as a function of eddy age. For the mid-ocean eddies in the region of BATS, (25°N–35°N and 295°E–305°E), the initial growth rate, defined here as the early stage of eddy growth during which the rate of change of eddy amplitude is positive and approaches zero, is estimated to be ≈8–9 weeks (Figure 4). This results in an estimate of 80–90 cm d^{-1} for the vertical velocities associated with eddy pumping in eddies near BATS. The vertical velocities associated with eddy intensification are expected to scale approximately linearly with eddy amplitude. Eddies in this region of the North Atlantic are of intermediate amplitude (mean and median amplitude of 8.4 and 6.8 cm, respectively) when compared with other midlatitude eddies observed globally [*Chelton et al.*, 2011b]. An eddy pumping velocity of $O(1\text{ m d}^{-1})$ likely represents a lower-bound estimate for eddies generated in energetic western boundary current regions and an upper-bound estimate for open ocean eddies.

The upwelling in cyclones and downwelling in anticyclones is a transient process, occurring during the early life stages of eddies and sometimes during eddy-eddy interactions. Decaying cyclones and anticyclones generate vertical velocities of the opposite sign: downwelling occurs in decaying cyclones and upwelling in decaying anticyclones [*Flierl and McGillicuddy*, 2002, cf. Figure 4.21]. In composite averages constructed from thousands of eddies, the CHL'' response to upwelling/downwelling occurring during eddy decay is indistinguishable from the CHL'' response to eddy-induced Ekman pumping, described in the next section.

The trend in CHL'' as a result of upwelling/downwelling during early life stages is expected to be positive in cyclones and negative in anticyclones, regardless of hemisphere and the ambient CHL gradient. In cyclones, CHL'' is expected to increase during intensification (Figure 3c, blue curve). The opposite is expected in anticyclones (Figure 3c, red curve). The idealized example presented here presumes that phytoplankton are only responding to upwelling and downwelling of nutrients during eddy intensification. This example reflects neither any changes in the composition of the phytoplankton community nor the influence of changes in predation.

A recent study of the life cycles of mesoscale eddies suggested that, following formation, eddy amplitude quickly increases during the first 15% of an eddy's lifespan [*Samelson et al.*, 2013]. After this initial rapid growth in amplitude, a transition to a slow-growth phase occurs that persists throughout the first half of the eddy lifespan. Our idealized conceptual model of the CHL'' response occurring during eddy intensification (Figure 3c) is consistent with these observations.

Observed time series of CHL'' in regions where eddy intensification dominates the phytoplankton response in eddies might not necessarily originate at zero as a result of the 1 cm amplitude threshold and closed contour of SSH criteria used to define eddies (see section 2.1). This ambiguity is shown schematically by the grey shading in Figure 3, which illustrates that the CHL'' response is not registered until the SSH threshold is met and the eddy is first identified by the automated eddy tracking procedure. Furthermore, processes such as eddy-eddy interaction can generate upwelling and downwelling as a result of changes in eddy amplitude. The CHL responses to these transient upwelling and downwelling events are not time-
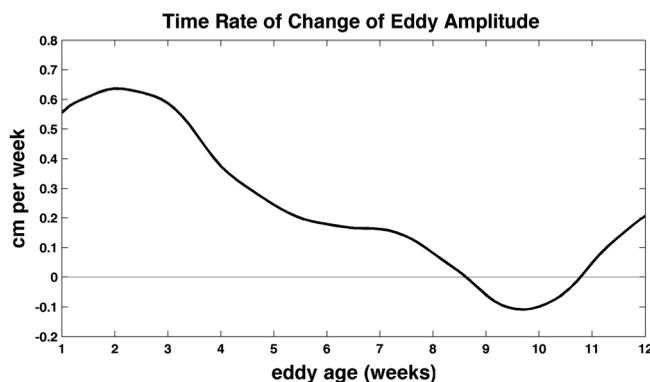
Figure 4. Time rate of change of the amplitude of eddies within the region 25°N–35°N and 295°E–305°E, which contains eddies similar to those observed at the Bermuda Atlantic Time series Study (BATS) site [*Siegel et al.*, 1999]. The amplitude time series was smoothed in time with a loess filter with a span of 30 days prior to computing the time rate of change. The location of the zero-crossing occurs at the same time in the unsmoothed time series.

synchronous with the different life stages of eddies and thus are not likely to be preserved in the aggregate time series and composites averages of CHL'' investigated in section 5.

3.4. Eddy-Induced Ekman Pumping

Unlike the transient vertical flux of nutrients occurring during eddy intensification, eddy-induced Ekman pumping results in upwelling in the cores of anticyclones and downwelling in cyclones during the entirety of an eddy's lifetime. Eddy surface current-induced Ekman pumping is generated by the surface currents associated with mesoscale ocean eddies, which impart a curl on the surface stress from the relative motion between air and water. This surface stress curl has a polarity opposite to that of the vorticity of the eddy, thus generating Ekman upwelling in the cores of anticyclones and downwelling in the cores of cyclones [*Dewar and Flierl*, 1987]. Eddy surface current-induced Ekman pumping downwells fluid out of the euphotic zone in cyclones (Figure 2d, bottom) and upwells nutrients from below the euphotic zone into the interiors of anticyclones (Figure 2d, top). In addition to the surface current-induced Ekman pumping, air-sea interaction associated with eddy-induced spatial variations of SST generate a wind stress curl and therefore Ekman pumping that is proportional to the crosswind SST gradient [*Chelton et al.*, 2004; *O'Neill et al.*, 2010; *Gaube et al.*, 2014]. Vertical velocities associated with total eddy-induced Ekman pumping from surface current and SST (W_E) are on average $O(10\,\mathrm{cm\ d^{-1}})$ globally [*Gaube et al.*, 2014], but can exceed $O(\sim 1\,\mathrm{m\ d^{-1}})$ in strong eddies at high wind speeds [*Martin and Richards*, 2001]. The W_E velocities reported here are a lower-bound estimate because of the space-time smoothing of the $\nabla \times \tau$ data. Extreme values of W_E can thus be of the same magnitude as vertical velocities associated with eddy intensification (see section 3.3).

Eddy-induced Ekman pumping was first hypothesized by *Martin and Richards* [2001] as a mechanism for sustaining an anomalous phytoplankton bloom observed in a mode-water type anticyclone in the North Atlantic Ocean. Shipboard surveys of another mode-type anticyclone in the Sargasso Sea confirmed the importance of eddy surface current-induced upwelling [*McGillicuddy et al.*, 2007]. Phytoplankton concentrations in the core of the anticyclone were eight standard deviations higher than the mean background field. Sulfur hexafluoride tracer released into the eddy core upwelled at a rate of $40\,\mathrm{cm\ d^{-1}}$, which was comparable to the W_E computed from only the wind and eddy surface current effects averaged over the time period of the tracer experiment [*Ledwell et al.*, 2008].

Eddy-induced Ekman pumping may also be responsible for enhanced CHL in regular anticyclones as well. From the analysis of satellite observations of thousands of long-lived anticyclones in the South Indian Ocean, *Gaube et al.* [2013] suggested that eddy-induced Ekman pumping may sustain positive CHL anomalies in the cores of anticyclonic eddies. Anticyclonic eddies in this region have been shown to have vertical structure consisting of downward displaced isopycnals within the eddy interior [*Feng et al.*, 2007; *Waite et al.*, 2007a]. To our knowledge, mode-water type eddies have not been documented in this region.

During the formation of a regular anticyclone, near-surface isopycnals are displaced downward, resulting in the downwelling of nutrient-depleted water. Time series observations at BATS seldom document nutrient-depleted waters in the aphotic zone (*McGillicuddy et al.*, 1999), suggesting that nutrients are replenished rapidly once an isopycnal is downwelled into the dark. However, the precise mechanisms by which nutrients are restored on isopycnals in the aphotic zone are not understood. In any case, it is possible that these nutrients can be upwelled back into the euphotic zone through the process of eddy-induced Ekman pumping, resulting in observable increases in CHL. It is important to note that targeted in situ studies have

not investigated the link between enhanced CHL and eddy-induced Ekman pumping in regular anticy-clones (as opposed to mode-water type eddies). It is therefore not possible to quantify the relative impor-tance of regular anticyclones and mode-water type eddies in driving the observed correlation between eddy-induced Ekman pumping and CHL anomalies in anticyclonic eddies.

During the initial intensification of eddies, CHL'' increases in anticyclones and decreases in cyclones as a result of the dependence of Ekman pumping on the vorticity of eddy surface currents, and consequently on the eddy amplitude (Figure 3d). As described in section 3.3, the true time of eddy origination is generally not the time at which an eddy is first detected by the eddy identification and tracking procedure. Therefore, in regions where ecosystems in eddies only respond to eddy-induced Ekman pumping, the CHL'' time series might not originate at zero. Following formation, CHL'' should remain positive in anticyclones and negative in cyclones. All else being equal, the magnitude of the CHL'' should decrease as the eddy decays and the associated W_E decreases.

Although the vertical velocities associated with W_E are, on average, small compared to those associated with eddy intensification, they are persistent throughout the lifetime of the eddy, varying in magnitude depending on eddy amplitude and the ambient wind speed [*Gaube et al.*, 2014]. In contrast, isopycnal dis-placements from eddy pumping are transient, with $O(1\,\mathrm{m}\,\mathrm{d}^{-1})$ vertical velocities occurring only during eddy intensification. Eddy-induced Ekman pumping therefore provides a mechanism by which enhanced CHL can be sustained in the cores of anticyclones long after their formation.

3.5. Manifestation of the Four Mechanisms in the Covariability of SSH and CHL

The regional response of the phytoplankton community to mesoscale eddies can be inferred from cross cor-relation of the SSH structure of eddies and their CHL'. The cross correlation at zero time lag (henceforth referred to as r'_0) provides insight into the response of CHL to SSH variability within the interiors of eddies. Time-lagged cross correlations provide insight into the response of CHL at the periphery of eddies where the rotational velocities of eddies are maximum, by virtue of the spatial offset between extrema of SSH and CHL' and the propagation speed and direction of the eddies.

The sign of r'_0 expected from the trapping of CHL during eddy formation depends on the nature of the ambient $\overline{CHL}$ gradient, the direction of the eddy-generating current (if there is one), and the rotational sense of the eddy. As described in section 2.3, the cross-current $\overline{CHL}$ gradient ($\partial\overline{CHL}/\partial n$) is computed from the mean geostrophic current and the background $\overline{CHL}$ gradient and is defined to be positive when increas-ing to the left of the mean geostrophic current looking downstream. For northern hemisphere cyclones formed in regions such as western and eastern boundary currents where $\partial\overline{CHL}/\partial n > 0$, the correlation r'_0 is expected to be negative. For southern hemisphere cyclones formed in regions where $\partial\overline{CHL}/\partial n < 0$, e.g., in the western boundary currents and all the eastern boundary currents except the Leeuwin Current off the west coast of Australia, the correlation r'_0 is also expected to be negative. Further combinations of eddy polarity and the sign of $\partial\overline{CHL}/\partial n$ are summarized in Table 1.

In regions where eddy intensification dominates the response of phytoplankton to mesoscale eddies, cyclonic eddies (with negative SSH) should contain positive CHL' in their cores and anticyclonic eddies (with positive SSH) should have negative CHL', both of which result in $r'_0 < 0$ (Table 1). In regions where W_E domi-nates the response of phytoplankton to mesoscale eddies, anticyclonic eddies would be associated with positive CHL' and cyclonic eddies with negative CHL', both of which result in $r'_0 > 0$.

It is evident from Table 1 that the sign of r'_0 does not provide unambiguous diagnosis of the underlying mechanism(s). For example, a CHL response to upwelling/downwelling occurring during eddy intensifica-tion cannot be differentiated from the trapping of CHL during eddy formation in regions where the ambient $\overline{CHL}$ gradient favors enhanced and suppressed CHL in the interiors of cyclonic or anticyclonic eddies, respectively. Likewise, a CHL response to W_E cannot be differentiated from the trapping of CHL in regions where the ambient $\overline{CHL}$ gradient favors enhanced and suppressed CHL in the interiors of anticyclonic and cyclonic eddies, respectively. The temporal evolution of the SSH and CHL signatures of eddies can help to address these ambiguities, as was discussed in sections 3.1–3.4 and will be further explored in section 5.

Eddy stirring results in CHL'' with an asymmetric dipole that is manifest in the time-lagged cross correlation of SSH and CHL' [*Chelton et al.*, 2011a]. A positive extremum of cross correlation occurs at a time lag that is greater than zero, corresponding to CHL' leading SSH. This is a result of westward propagation of

midlatitude eddies in most regions and the fact that the leading (western) pole of the CHL'' (or CHL') is larger in magnitude than the trailing pole. A secondary negative extremum of the cross correlation occurs at negative lags with magnitude smaller than the positive cross-correlation extremum at positive lags because of the smaller amplitude and opposite sign of the trailing pole.

To choose an appropriate time lag, we examined previously published composite averages of midlatitude CHL' [*Chelton et al.*, 2011a] to identify the distance from the eddy center where the CHL' response to horizontal eddy surface currents is strongest. The CHL' anomaly extrema of midlatitude eddies are located at a distance of approximately L_s from the eddy centroid [*Chelton et al.*, 2011a], which corresponds to ∼70–110 km in midlatitude eddies, with L_s generally decreasing with increasing latitude [*Chelton et al.*, 2011b]. The typical westward propagation speed of midlatitude eddies is ∼2–6 cm s^{-1}, again decreasing with increasing latitude [*Chelton et al.*, 2011b]. From these estimates and the fact that the strong cross correlation between SSH and CHL' occurs along the western edge of the westward propagating eddies, maximum cross correlation is expected at a positive time lags ranging from 3 to 7 weeks. In this study, we consider the cross correlation at a positive lag of 4 weeks (henceforth referred to as r_4'). In some regions, cross correlation at positive time lags other than 4 weeks is slightly larger in magnitude than r_4', but to simplify for the present analysis we consider only a lag of 4 weeks. The results presented in section 4 are qualitatively similar when considering cross correlation at time lags ranging from 2 to 8 weeks. A summary of the expected sign of r_4', as a function of direction of eddy rotation and the meridional $\overline{CHL}$ gradient is provided in Table 1.

It should be noted that r_4' is not an appropriate metric to assess the influence of eddy stirring in regions of eastward propagating eddies, such in the Antarctic Circumpolar Current, Gulf Stream, and Kuroshio Extension [*Chelton et al.*, 2011b].

4. Global Observations of the Response of Phytoplankton to Mesoscale Eddies

4.1. Overall Patterns of CHL and SSH Covariability

From a global overview of the zero-time-lagged CHL response to mesoscale eddies (Figure 1a), it can be observed that both the sign and the magnitude of the CHL response to eddy amplitude vary regionally, with some regions characterized by positive r_0' and others by negative r_0'. Globally, 15% and 30% of long-lived eddies occur in regions of significantly positive and negative r_0', respectively. This factor-of-2 difference is primarily a result of twice as much ocean surface having negative versus positive r_0' (13% and 26%, respectively).

Negative r_0' is observed in all western boundary current systems and their midlatitude extensions, including the Kuroshio Current, the Agulhas Current, the Gulf Stream, the Brazil-Malvinas Confluence, and the East Australia Current. Similarly, most eastern boundary current systems, such as the California Current, the Peru-Chile Current, and the Benguela Current, are characterized by negative r_0'. An exception is the Leeuwin Current, a poleward-flowing eastern boundary current off the western coast of Australia, which is characterized by positive r_0' that extends nearly all the way across the South Indian Ocean. Regions of positive r_0' are also observed in the central South Pacific, subtropical North and South Atlantic and around the Hawaiian Islands in the central North Pacific. Regions of negative r_0' are observed in open ocean regions, such as northeast of Madagascar and to the east of the Hawaiian Islands in the North Pacific.

To investigate whether the observed r_0' in any particular region is predominately a result of a CHL response to cyclonic or anticyclonic eddies, the cross-correlation coefficient was computed separately for eddies of each polarity. From the separate maps (Figures 1b and 1c), we conclude that the observed r_0' is primarily a result of a CHL' response to cyclonic eddies in the Gulf Stream, Brazil-Malvinas, and California Current systems, as well as the region south and east of the Hawaiian Islands. The positive r_0' observed in the central South Pacific, however, appears to be generated by a CHL' response in eddies of both polarities.

4.2. Vertical Transport

In the map of r_0' (Figure 1a), we can identify regions where the response of phytoplankton could reflect the expected response to vertical nutrient fluxes during eddy intensification. Particularly, strong negative r_0' values are observed in most western and eastern boundary currents along with their midlatitude extensions. Western boundary currents are generally associated with energetic, large-amplitude mesoscale eddies [*Chelton et al.*, 2011b] and therefore a response of the phytoplankton communities to eddy intensification is expected, assuming that the vertical velocities associated with eddy intensification scale linearly with eddy

amplitude. Furthermore, the majority of the observed negative r'_0 arises from negative CHL' in cyclonic eddies (Figure 1c), which is consistent with upwelling in cyclones during intensification and also the trapping of coastal waters in these regions, which have higher CHL. The generally less negative, and sometimes positive r'_0 in anticyclones in most energetic western boundary current regions (Figure 1b) could result from a phytoplankton response to eddy-induced Ekman pumping which provides a slow, yet persistent, upwelling in anticyclones throughout their lifetimes.

Regional variability in the response to eddy-induced Ekman pumping can be observed in a map of the cross correlation of CHL' with W_E (henceforth referred to as r'_E, Figure 1d). Regions where enhanced CHL' is associated with Ekman upwelling and suppressed CHL' with Ekman downwelling result in $r'_E > 0$. As described in section 3.4, anticyclones are associated with surface current-induced Ekman upwelling and cyclones with downwelling. Regions of significant r'_E therefore tend to be collocated with regions of significant r'_0 of the same sign (cf. Figures 1a and 1d). The largest region of $r'_E > 0$ is the South Indian Ocean, which is explored in section 5.5 and by *Gaube et al.* [2013]. Smaller regions of $r'_E > 0$ are found in the tropical Pacific and Atlantic Oceans. We note that there are several small regions for which r'_E is negative. We do not have a mechanistic model to explain $r'_E < 0$, and therefore surmise that CHL variability in those regions is dominated by some unknown process that is negatively correlated with W_E. As such, we interpret these $r'_E < 0$ correlations as non-causal.

4.3. Trapping

The trapping of CHL during eddy formation may also have an imprint on maps of r'_0. In the northern hemisphere in regions where $\partial \overline{CHL}/\partial n$ is positive, we expect to find negative r'_0 associated with this process. The collocation of negative r'_0 with positive $\partial \overline{CHL}/\partial n$ is observed in all northern hemisphere western and eastern boundary current systems (Figure 5b). Likewise, southern hemisphere western and eastern boundary current systems (except for the Leeuwin Current System) are associated with negative r'_0 and negative $\partial \overline{CHL}/\partial n$, as expected from the anticipated r'_0 described in Table 1.

In some regions of the northern hemisphere, such as north and south of the Hawaiian Islands and in the Alaska Current, positive r'_0 is collocated with negative $\partial \overline{CHL}/\partial n$ (Figure 5b). In the southern hemisphere, positive r'_0 is collocated with positive $\partial \overline{CHL}/\partial n$ to the southeast of New Zealand, to the south of the Agulhas Retroflection, and most notably, in the region west of the Leeuwin Current in the interior South Indian Ocean, where positive $\partial \overline{CHL}/\partial n$ is almost exactly collocated with significantly positive r'_0. The sign of r'_0 in these areas is again consistent with expectation as described in Table 1.

4.4. Stirring

Long swaths of significant r'_4 (the cross correlation of SSH and CHL' at 4 weeks lag) are observed in the mid-latitude oceans (Figure 6a). These regions are associated with large meridional gradients of $\overline{CHL}$ (Figure 6b). For example, in the North Atlantic, the two bands of r'_4 with opposite sign are located within areas with meridional $\overline{CHL}$ gradients that are large in magnitude and also opposite in sign. In the northern hemisphere, negative r'_4 is generally collocated with positive meridional $\overline{CHL}$ gradients ($\overline{CHL}$ increasing northward) and positive r'_4 with negative meridional $\overline{CHL}$ gradients ($\overline{CHL}$ increasing southward). In the southern hemisphere, this correspondence between r'_4 and the sign of the meridional $\overline{CHL}$ gradients is reversed as a result of the opposite direction of rotation for cyclones and anticyclones. The salient features of r'_4 and the meridional $\overline{CHL}$ gradient observed in the Atlantic, Pacific, and South Indian Oceans are a result of the rotational advection of the ambient CHL gradient around eddies (see section 3.1 and Figure 2a).

The dominance of the azimuthal advection previously documented for near-surface $\log_{10}(CHL)$ around midlatitude eddies [*Chelton et al.*, 2011a] is also observed globally in anomalies of non-log transformed, normalized CHL anomalies (CHL''). This is apparent from composite averages of CHL'' constructed in a rotated coordinate system that aligns the ambient $<CHL>$ gradient to a polar angle of $\pm 90°$, as described in section 2.4. For eddies rotating clockwise in a northward $<CHL>$ gradient, the leading (westward) pole has negative CHL'' (Figure 7a, left). The northward velocity on the western side of the clockwise-rotating eddy advects low CHL water from the southwestern quadrant to the northwestern quadrant, resulting in negative CHL'' in the northwestern quadrant. The clockwise-rotating surface currents on the trailing edge advect relatively high CHL water from the northeastern quadrant to the southeastern quadrant, resulting in positive CHL'' in the southeastern quadrant. The opposite is true for clockwise-rotating eddies propagating in regions with a southward
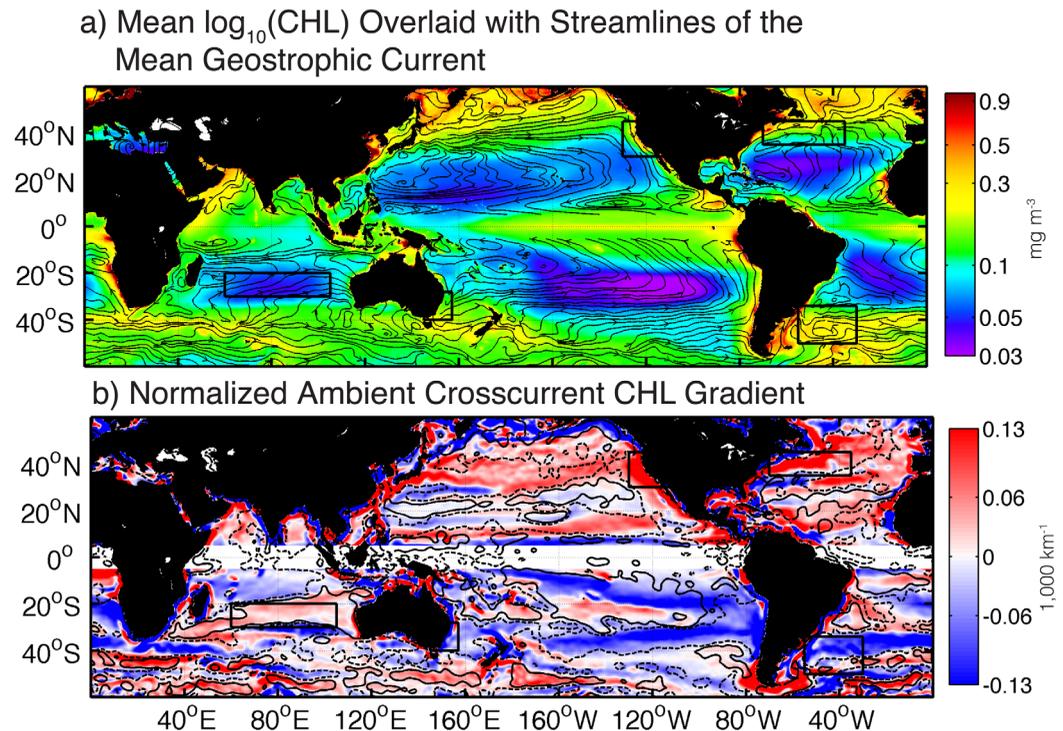
a) Mean log$_{10}$(CHL) Overlaid with Streamlines of the Mean Geostrophic Current

b) Normalized Ambient Crosscurrent CHL Gradient

Figure 5. (a) Map of the 13 year time-averaged $\overline{CHL}$ overlaid with streamlines of the mean geostrophic current computed from the AVISO absolute dynamic topography, averaged over the same time period. (b) Map of the normalized cross-current $\overline{CHL}$ gradient (see section 2.3 for the detail of how $\partial \overline{CHL}/\partial n$ is calculated and normalized) overlaid with contours of significant r_0' from Figure 1a. Positive cross-correlation coefficients are enclosed by a solid contour and negative by a dashed contour. The black boxes in Figures 5a and 5b enclose the five study regions investigated in section 5.

increasing background $<CHL>$ gradient (Figure 7b, left). Similar advective processes interacting with the CHL gradient produce the observed patterns in counterclockwise-rotating eddies (right of Figure 7).

As discussed in section 3.1, CHL'' on the leading (western) side of westward-propagating eddies is larger in magnitude than on the trailing (eastern) side (Figure 7). This structure is expected as a result of the trailing side of the eddy encountering a background field that has recently been perturbed by the leading side, as shown by *Chelton et al.* [2011a] from a model simulation of mesoscale eddies propagating through a passive tracer fluid with a meridional gradient.

5. Regional Variability of the Response of Phytoplankton to Mesoscale Eddies

In the regional analyses that follow, we investigate the spatial structure and time evolution of CHL'' in eddy-centric coordinates in an attempt to distinguish among the multiple mechanisms that can account for the observed response of CHL to mesoscale eddies in each region. As discussed in section 2.3, CHL'' has been normalized by the time-averaged background CHL ($\overline{CHL}$). Comparisons of the magnitudes of eddy-induced CHL'' computed for different regions are therefore not advised.

The five regions examined below were chosen because they exhibit significant CHL responses to eddies as quantified by significant r_0' in Figure 1a. These regions include western boundary currents in both hemispheres, an eastern boundary current, and an open ocean region. Together, the results presented in sections 5.1–5.5 provide examples of each of the four mesoscale physical/biological mechanisms discussed in section 3.

The Gulf Stream, Brazil-Malvinas Confluence, and East Australia Current are western boundary currents that were chosen because they generate energetic eddies that represent the upper tenth percentile for largest eddy amplitudes globally and are characterized by significant negative r_0'. In these western boundary currents, eddies entrain elevated or suppressed CHL into the interiors of cyclones or anticyclones, respectively. The California Current System was chosen as an example eastern boundary current that generates long-
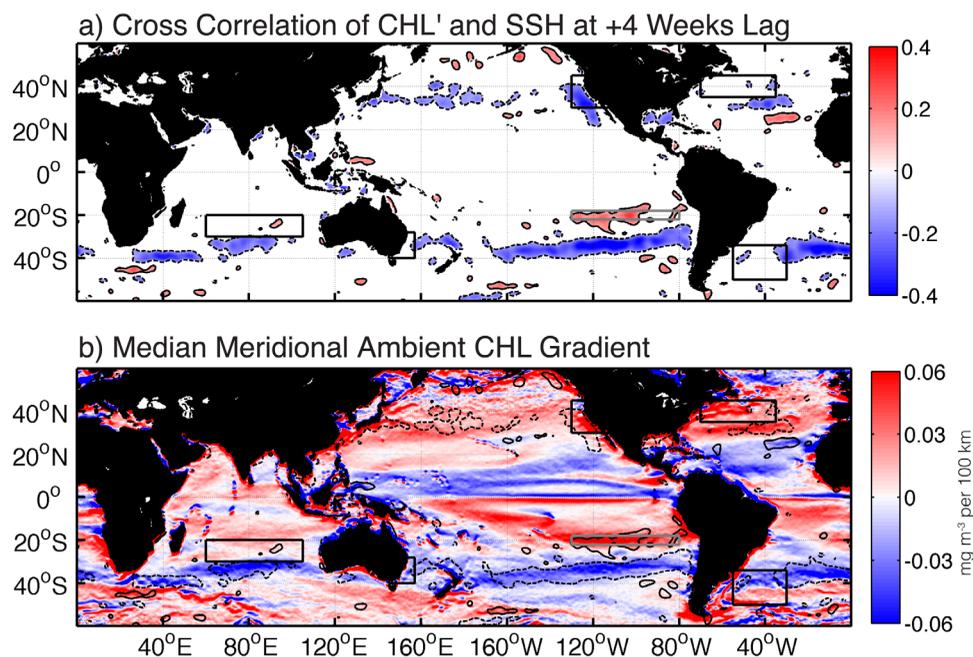
Figure 6. (a) Map of the cross correlation of CHL' and SSH at a time lag of $+4$ weeks (r'_4, CHL' leads SSH). Lagged cross-correlation coefficients that are significantly positive at $\alpha=0.05$, $r'_4 \geq 0.09$ are enclosed by a solid contour, $r'_4, \leq -0.09$ are enclosed by the dashed contour. White areas correspond to correlations smaller than the estimated 95% significance level, computed as described in the caption of Figure 1. (b) The median meridional $\overline{CHL}$ gradient (positive values are northward and negative values are a southward). The same contours shown in Figure 6a are overlaid on Figure 6b. The black boxes in all figures enclose the five study regions investigated in section 5 and the grey box encloses the domain investigated by *Chelton et al.* [2011a].

lived eddies propagating far into the interior Pacific Ocean. Eddies in the California Current System are associated with significant negative r'_0 and entrain elevated or suppressed CHL into the interiors of cyclones or anticyclones, respectively. Finally, the interior South Indian Ocean was chosen because it exhibits a global maximum in r'_E. *Gaube et al.* [2013] have previously shown that a CHL response to W_E is observed in this region. Furthermore, South Indian Ocean eddies entrain elevated or suppressed CHL into the interiors of anticyclones or cyclones, respectively, which is opposite that of the other four regions. There are, however, many other regions that display significant r'_0, which will be evaluated in future investigations.

5.1. The Gulf Stream

The region around the Gulf Stream (GS), defined here as 35°N–45°N and 290°E–325°E, generates energetic mesoscale eddies with a general tendency for cyclonic cold-core rings and anticyclonic warm-core rings to pinch off of the southern and northern sides of the GS, respectively (Figure 8a). The horizontal speed-based scale L_s of eddies generated in this region is about the same for each polarity ($L_s \approx 90$ km, Table 2). However, the average amplitude of cyclones is 28.7 cm, which is more than 50% larger than the anticyclones that have an average amplitude of 17.9 cm. It is noteworthy that the subset of eddies analyzed here likely also includes some mid-ocean eddies that are not GS rings.

The observed negative r'_0 in this region (Figure 1a) results primarily from the CHL response in cyclones, and to a lesser extent in anticyclones (Figures 1b and 1c). As expected from this negative correlation, the composite averages of CHL'' and SSH of these GS eddies reveal that cyclonic GS eddies contain positive CHL'' and anticyclonic GS eddies contain negative CHL'' in their interiors (Figure 9a). In contrast to the composite averages constructed from all midlatitude eddies (Figure 7), GS eddies are best described as monopole CHL'' structures. There are two primary mechanisms that can result in elevated CHL'' in the cores of cyclones and depressed CHL'' in the cores of anticyclones: the trapping of CHL during eddy formation (see section 3.2) and upwelling/downwelling that occurs during eddy intensification (see section 3.3).

Based on r'_0 and the eddy-centric composites, we are not able to distinguish between these two processes. The evolution of the SSH amplitudes of eddies and their CHL'' can provide insight into whether the observed CHL response is influenced by vertical nutrient and CHL fluxes during eddy intensification. A
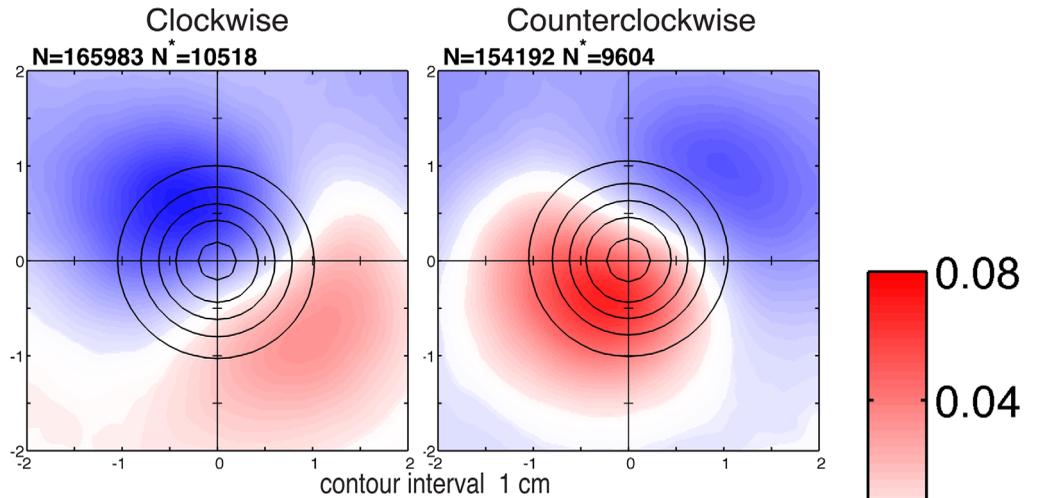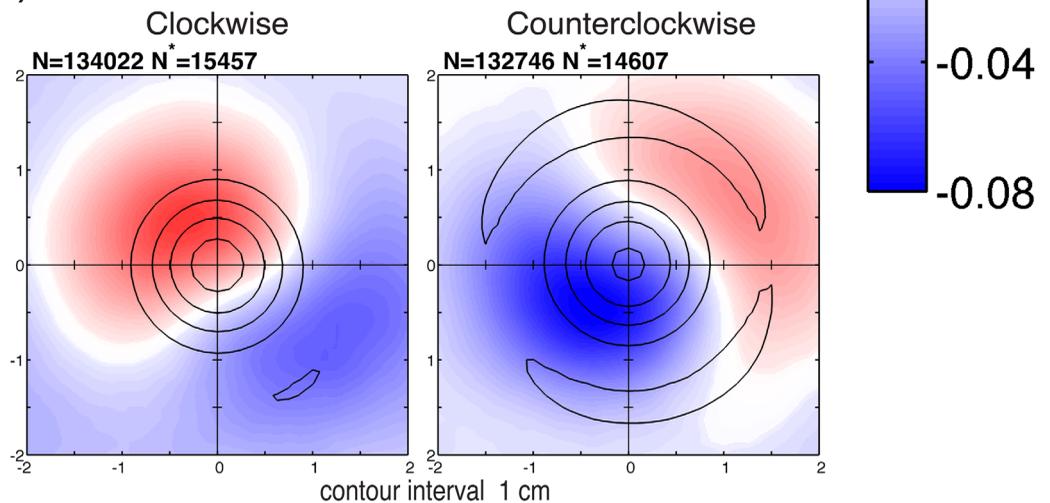
Figure 7. Global composite averages of CHL'' overlaid with contours of $|SSH|$ for eddies propagating through a (a) northward background $<CHL>$ gradient and (b) a southward background $<CHL>$ gradient. Each eddy observation used to construct Figures 7a and 7b was rotated to align the background $<CHL>$ gradient to a polar angle of either $\pm 90°$ prior to the construction of the composites (see section 2.4). Regions of the composite that do not exceed the 95% confidence interval of mean are masked with white. The 95% confidence interval for the mean is defined as $\pm \sigma(x, y) q_t (0.025, N^* - 1)/\sqrt{N^*}$ where $\sigma(x, y)$ is the standard deviation of the CHL'' estimates at any particular location within the composite average and $q_t(0.025, N^* - 1)$ is the 2.5 percentage point of the Student's t distribution with $N^* - 1$ degrees of freedom, i.e., the numerical value that a Student's t random variable with $N^* - 1$ degrees of freedom exceeds with 2.5% probability. We used a conservative estimate of N^* as the number of long-lived eddies (lifetimes ≥ 12 weeks), which is far smaller than the number of eddy realizations N, from which the composites were computed. The title of each composite averages indicates both the number of eddy realizations N used to construct the composite and the effective degrees of freedom N^* used to compute the 95% confidence interval. The x and y coordinates of the composite averages are normalized by the eddy scale L_s, defined in the text.

statistically significant positive trend in CHL'' can be observed during the first 12 weeks of the lifetimes of GS cyclones (Figure 10a), suggesting that a CHL response to upwelling occurs during their intensification. No significant trends in CHL'' are observed in GS anticyclones.

The relationship between the GS and the ambient CHL field is such that high and low CHL is trapped in cyclones and anticyclones, respectively, during formation (Figure 5b). This is consistent with CHL'' being greater than and less than zero at the time of formation of cyclones and anticyclones, respectively (Figure 10a). From these observations, it can be concluded that both the trapping of CHL during formation and
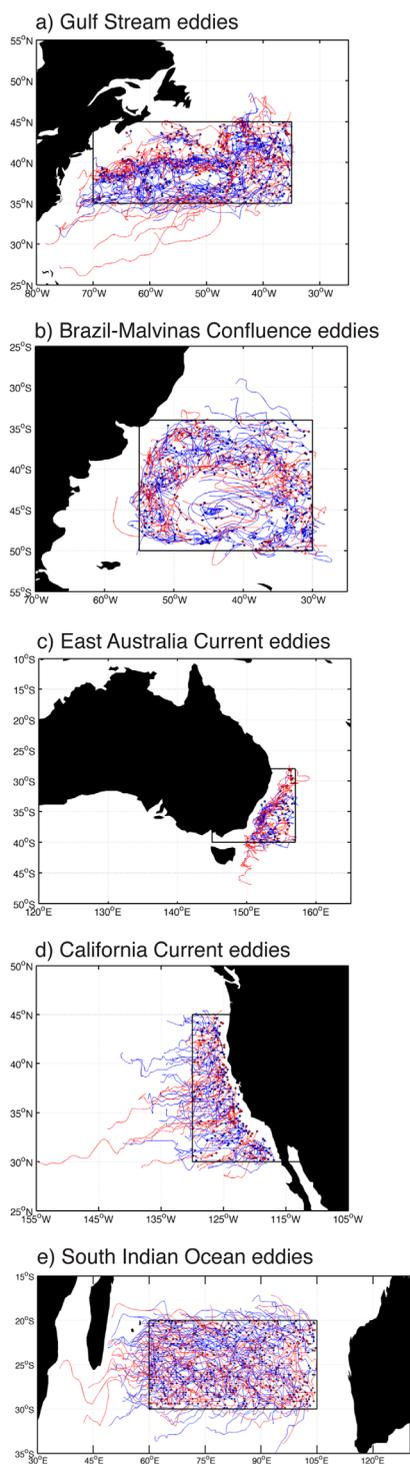
Figure 8. Trajectories of the long-lived mesoscale eddies (lifetimes ≥ 12 weeks) used to construct the composites shown in Figure 9. Anticyclones are shown in red and cyclones in blue. The location of origination is shown as a black point for each eddy trajectory. (a) Gulf Stream eddies, (b) Brazil-Malvinas Confluence eddies, (c) East Australia Current eddies, (d) California Current System eddies, and (e) interior South Indian Ocean eddies. The latitude and longitude bounds of eddy formation locations for each of the regions are enclosed by a black box in each figure and listed in Table 2.

upwelling generated during intensification result in the observed positive CHL'' in GS cyclones. The CHL response to GS anticyclones appears to be dominated by the trapping of water that is low in nutrients and phytoplankton concentration during eddy formation.

5.2. The Brazil-Malvinas Confluence

The Brazil-Malvinas Confluence (BMC), defined here as 34°S–50°S and 305°E–330°E (Figure 8b), is a region of active eddy generation that spawns large-amplitude cyclones and anticyclones that have mean amplitudes of 20.4 and 18.0 cm, respectively (Table 2). The BMC is a region where both r_0' and $\partial \overline{CHL}/\partial n$ are strongly negative (Figure 5b). Similar to the GS region considered in section 5.1, composite averages of CHL'' in BMC eddies reveal that the spatial structure of CHL'' consists primarily of monopoles of high CHL'' in cyclones and low CHL'' in anticyclones (Figure 9b) that are nearly centered on the eddy SSH extrema. This spatial structure is again consistent with both a CHL'' response to the trapping of CHL and nutrients during eddy formation and a vertical flux of nutrients and CHL during eddy intensification. Specifically, BMC cyclones and anticyclones have positive and negative CHL'' at the time of formation (Figure 10b), indicative of the trapping of CHL during eddy formation. The positive trend in CHL'' during the first 12 weeks of the lifetimes of BMC cyclones (Figure 10b) suggests a near-surface CHL'' response to vertical velocities generated during eddy intensification. Similar to the GS rings considered above, significant trends in CHL'' are not observed in BMC anticyclones, suggesting that the observed negative CHL'' originates from the trapping of water low in nutrients and CHL during eddy formation.

5.3. The East Australia Current

The third western boundary current system investigated here is the East Australia Current (EAC) that flows poleward along the east coast of Australia. For this analysis, we define EAC eddies as being generated in the region 28°S–40°S and 145°E–157°E. The EAC generates large-amplitude eddies (mean amplitude of 22 and 23 cm for cyclones and anticyclones, respectively; see Table 2) that are advected southward by the EAC (Figure 8c). The EAC region is characterized by significant negative values of both r_0' and $\partial \overline{CHL}/\partial n$, suggesting that cyclones trap elevated CHL and anticyclones trap suppressed CHL, which is observed in the composite averages of CHL'' (Figure 9c). A survey of an individual anticyclonic eddy generated by the EAC

Table 2. Overview of Mesoscale Eddy Statistics for Each of the Five Study Regions for the 9 Year Period January 2001 Through November 2009, During Which Concurrent Measurements of Ocean Color, SSH, and Vector Winds Are Available[a]

	Gulf Stream	Brazil-Malvinas Confluence	East Australia Current	California Current System	South Indian Ocean
Latitude	35°N–45°N	34°S–50°S	28°S–40°S	30°N–45°N	20°S–30°S
Longitude	290°E–325°E	305°E–330°E	145°E–157°E	230°E–250°E	60°E–105°E
N eddies	243/209	242/175	41/45	130/117	304/222
N realizations	5109/3683	4361/2912	825/1037	3039/2674	6819/5916
Amplitude (cm)	28.7/17.9	20.4/18.0	21.8/23.1	6.4/4.9	7.2/7.7
Scale (km)	89/91	90/96	92/97	85/82	104/105
Axial speed (cm s^{-1})	47.5/34.2	33.8/32.3	43.1/45.8	14.4/12.5	19.5/19.8

[a]Values shown in rows 3–7 are reported as cyclones/anticyclones. Mean values are shown in rows 5–7.

identified a case of the latter: a lens of nutrient-depleted surface water trapped in the eddy core during formation [*Andrews and Scully-Power*, 1976].

Composite time series of CHL'' (Figure 10c) add further support for the importance of the trapping of CHL during eddy formation in the EAC. Specifically, CHL'' is greater than and less than zero at the time of first detection of cyclones and anticyclones, respectively. Temporal trends in CHL'' are not statistically significant in EAC eddies.

5.4. The California Current System
The California Current System (CCS) is an eastern boundary current system with generally equatorward flow at the surface (except for poleward flow very nearshore in winter) that generates mesoscale eddies that are much smaller in amplitude than the eddies observed in western boundary current systems (the mean amplitudes of cyclones and anticyclones are 6.4 and 4.9 cm, respectively). For this study, the CCS region is defined as 30°N–45°N and 230°E–250°E (Figure 8d). The longest-lived anticyclone propagated more than 3200 km to the west from its point of origin in the CCS during its ∼4 year lifetime.

The composite averages of CHL'' in CCS eddies have spatial structures that can be described as asymmetric dipoles (Figure 9d). In CCS cyclones, a primary pole of elevated CHL'' is located slightly west-northwest of the eddy SSH extremum and a weak secondary pole of negative CHL'' is located to the southeast of the SSH extremum (Figure 9d, right). Anticyclones in the CCS contain a primary pole of negative CHL'' that is displaced to the northeast of the eddy SSH extremum and a weak secondary pole of positive CHL'' located to the south-southwest of the eddy SSH extremum (Figure 9d, left). These spatial structures of the CHL'' composites are consistent with the expected structures resulting from (1) the advection of the ambient CHL gradient (low offshore, high nearshore; Figure 5a) around the eddy peripheries, (2) the trapping of CHL during eddy formation, and (3) a CHL response to vertical velocities generated during eddy intensification.

The time evolution of CHL'' in CCS eddies suggests that on average, the trapping of elevated CHL is observed, as evidenced by the fact that CHL'' in both cyclones and anticyclones is initially significantly different from zero (positive and negative in cyclones and anticyclones, respectively; Figure 10d). In CCS cyclones, an initial increase in CHL'' is observed during the first 3 weeks of their lifetimes, suggesting a CHL'' response to upwelling during eddy intensification. The difference in CHL'' between weeks 1 and 3 is, however, not significant. It thus appears that the observed CHL'' of CCS eddies is a result of both the stirring of the ambient CHL field and the trapping of CHL during eddy formation. It is important to note, however, that a CHL response to vertical velocities occurring during the intensification of CCS eddies might occur near the base of the euphotic zone, too deep to be observed in satellite measurements of ocean color.

5.5. The Interior South Indian Ocean
The CHL anomalies of Southern Indian Ocean eddies have been studied in detail by *Gaube et al.* [2013]. In the present study, we consider only a subset of South Indian Ocean (SIO) eddies in the region of particularly strongly positive r'_E in the interior Indian Ocean beyond the direct influence of the Leeuwin Current (Figure 1d). This subset, referred to here as interior SIO eddies, is defined as having originated in the region 20°S–30°S and 60°E–105°E (Figure 8e).

It has been shown that anticyclones formed in the Leeuwin Current preferentially entrain nutrient-rich and CHL-rich coastal waters during formation [*Pearce and Griffiths*, 1991; *Moore et al.*, 2007; *Waite et al.*, 2007b].

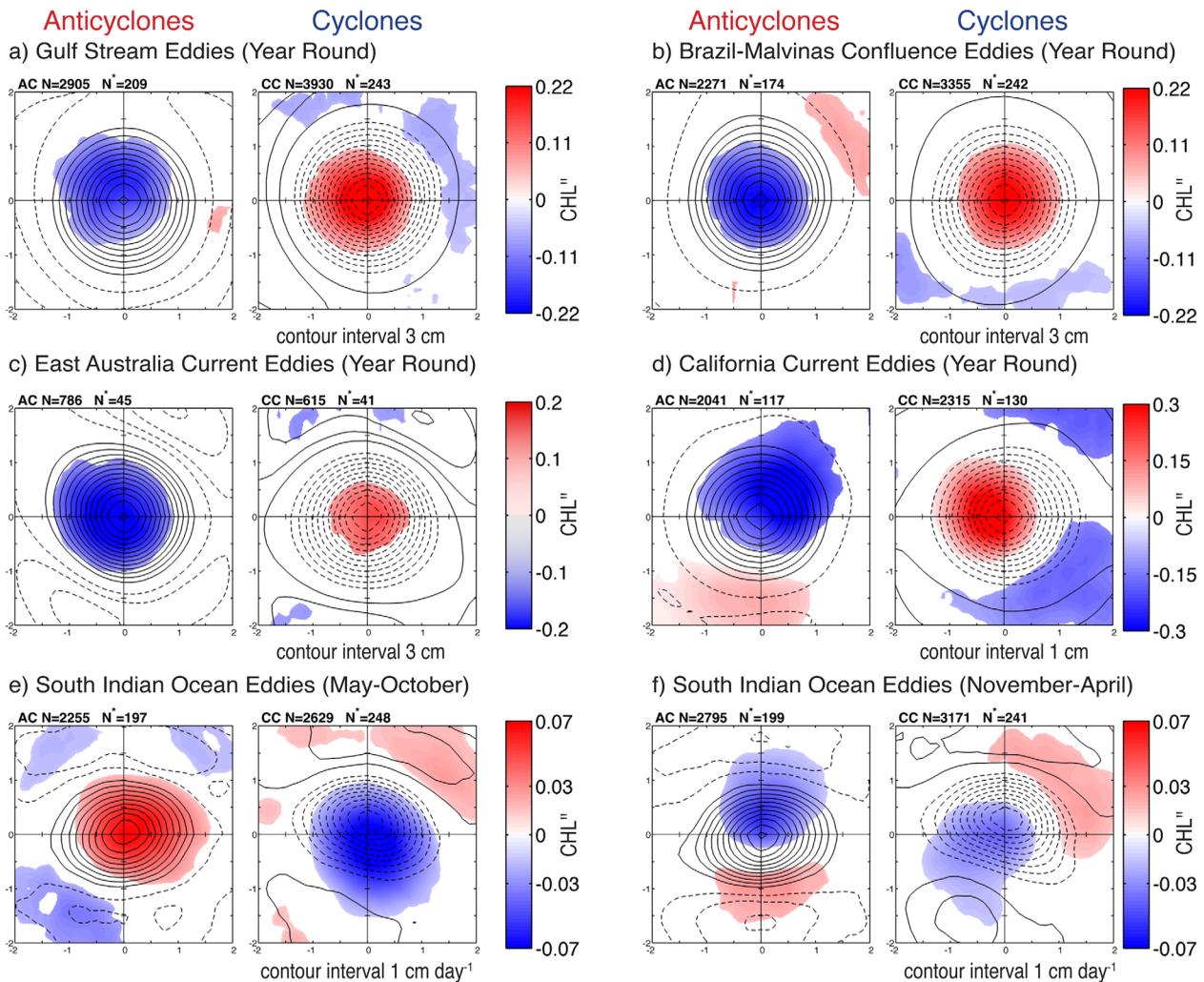## Composite Averages of Normalized CHL Anomalies (CHL")

Figure 9. Composite averages of *CHL″* overlaid with (a–d) contours of the composite average SSH and (e and f) eddy-induced Ekman pumping. Figure 9a shows Gulf Stream eddies; Figure 9b, Brazil-Malvinas Confluence eddies; Figure 9c, East Australia Current eddies; Figure 9d, California Current System eddies; Figure 9e, interior South Indian Ocean eddies computed from observations made during the months of May through October; and Figure 9f, interior South Indian Ocean eddies computed from observations made during the months of November through April. Regions of the composite that do not exceed the 95% confidence interval of mean are masked with white. The 95% significance level was computed as described in the caption of Figure 7. The *x* and *y* coordinates of the composite averages are normalized by the eddy scale L_s. The title of each composite averages indicates both the number of eddy realizations *N* used to construct the composite and the effective degrees of freedom $N*$ used to computed the 95% confidence interval. The latitude and longitude bounds of each of the regions are shown in Table 2.

Eddies generated in the interior SIO, away from the influence of the Leeuwin Current, have been observed to preferentially entrain elevated and suppressed CHL and nutrients into anticyclones and cyclones, respectively [see Appendix B of *Gaube et al.*, 2013]. This is consistent with positive $\partial\overline{CHL}/\partial n$ in the interior SIO region (Figure 5b). May through October composite averages of *CHL″* in the SIO are characterized by positive values in the cores of anticyclones and negative values in the cores of cyclones, collocated with W_E of the same sign (Figure 9e). These patterns are consistent with the trapping of CHL during eddy formation and a subsequent *CHL″* response to W_E. Composite averages of *CHL″* in the SIO constructed from observations during November through April have dipole structures indicative of eddy stirring (Figure 9f). Such seasonal differences in spatial patterns of the eddy-centric composites do not occur in other regions. Consequently, only the year-round fields are presented in Figures 9a–9d.

As discussed in *Gaube et al.* [2013], the seasonal difference in spatial structure of *CHL″* in the eddies of the interior SIO is likely a result of basin-wide changes in stratification and the summertime development of a deep CHL maximum. During winter, deeper mixed layers cause near-surface waters to be more indicative of
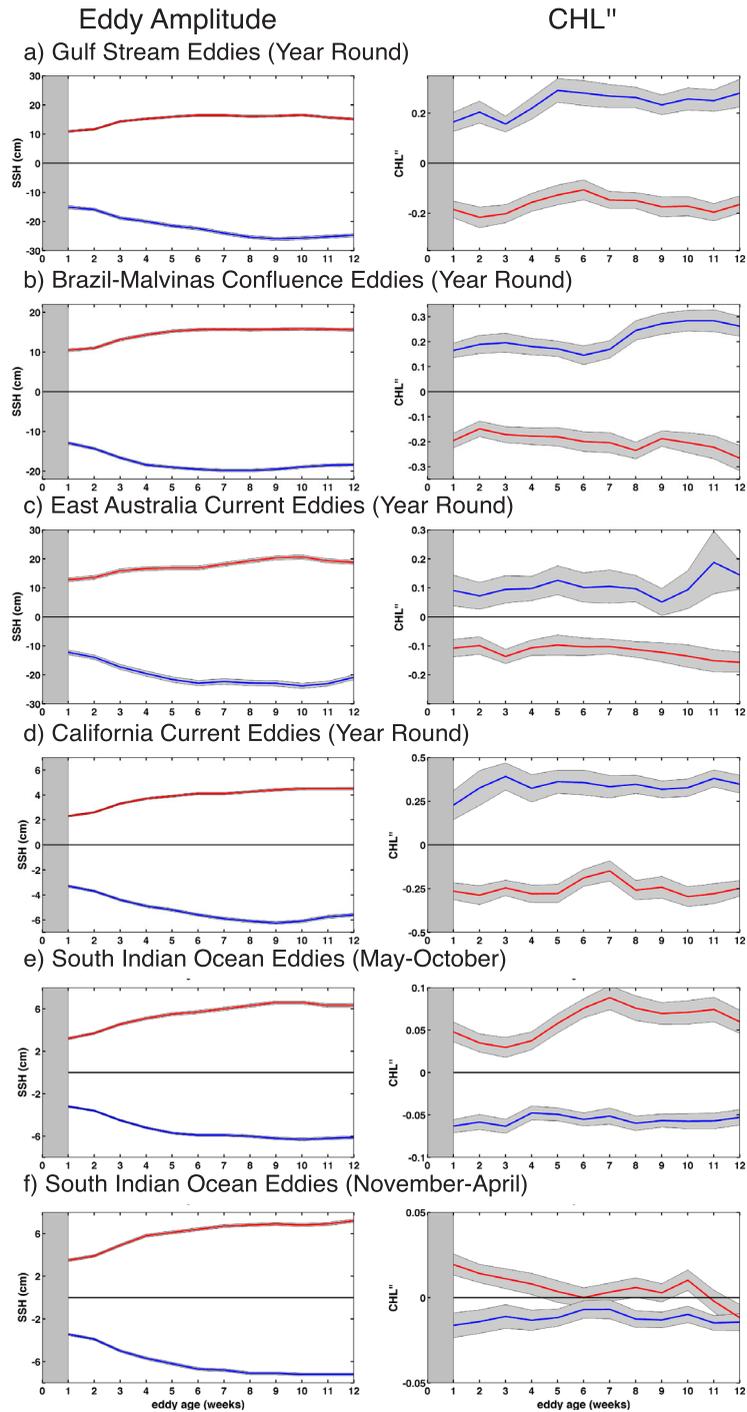
Figure 10. Composite average time series of (left) amplitude and (right) CHL'', bin averaged as a function of eddy age for (a) Gulf Stream eddies, (b) Brazil-Malvinas Confluence eddies, (c) East Australia Current eddies, and (d) California Current System eddies and (e) interior South Indian Ocean eddies computed from observations made during the months of May through October and (f) interior South Indian Ocean eddies computed from observations made during the months of November through April. The CHL'' time series are constructed from weekly, horizontally normalized CHL'' observations at the normalized x and y coordinates where the composite averages are identified as statistically significantly and within a radial distance of L_s of the eddy SSH extremum (see section 2.4). Anticyclones are shown in red and cyclones in blue with the standard error of the mean enclosed by grey shading. The standard error is defined as $\pm\sigma(k)/\sqrt{N(k)}$ where $\sigma(k)$ is the standard deviation of the spatially averaged CHL'' used to compute the k weekly averages and $N(k)$ is the number of eddy realizations in each weekly average. As in Figure 3, the beginning of the time series are shaded to indicate that both eddy amplitude and CHL'' are only observed after the eddy is first detected by the automated eddy tracking procedure, defined here as week 1.

dynamics occurring throughout the euphotic zone, permitting satellite observations of a response to eddy-induced Ekman pumping in interior SIO eddies (Figure 9e). On the other hand, during the summer, shallow mixed layers isolate near-surface waters from the nutricline below, so a CHL response to eddy-induced Ekman pumping would occur near the base of the euphotic zone, which is deeper than the first optical depth and thus more difficult to detect by satellites [*McGillicuddy et al.*, 2007; *Siegel et al.*, 2007; *Gaube et al.*, 2013]. Summertime composites of CHL'' in interior SIO eddies are therefore dominated by the stirring of CHL around eddies, resulting in CHL'' dipoles (Figure 9f).

Following the formation of anticyclones in the interior SIO, W_E appears to sustain and enhance the positive CHL'' trapped in anticyclones. This can be seen in the time evolution of CHL'' constructed from observations made from May through October (Figure 10e), where CHL'' in SIO anticyclones is observed to be significantly elevated during weeks 6–11 compared with weeks 1–4. During the Austral summer (Figure 9f), interior SIO anticyclones and cyclones also contain positive and negative CHL'', respectively, at the time of first detection. These summertime differences in the sign of CHL'', however, become less significant later in the time series.

6. Conclusions

Global observations of SSH and CHL reveal that the mechanisms by which eddies influence marine phytoplankton vary regionally. At any given time and location, the CHL within an eddy can be influenced by one or more of the above biophysical processes. The response of phytoplankton to eddies (inferred from composite averages of the eddy-centric normalized CHL anomalies) can be attributed to (1) the horizontal advection ("stirring") of phytoplankton around the peripheries of eddies, (2) the transport of ecosystems in the trapped cores of eddies, (3) upwelling and downwelling, and (4) eddy-induced changes in stratification. The latter was shown in this study to only impact eddy-induced CHL anomalies in the interior SIO, where seasonal variations in the CHL response to eddies were observed. The influence of eddies on stratification and CHL in the SIO has been investigated in detail by *Gaube et al.* [2013].

A recent analysis of the influence of midlatitudes eddies on $\log_{10}$ transformed CHL showed that the globally dominant mechanism by which eddies influence CHL is the azimuthal advection of CHL around eddy peripheries [*Chelton et al.*, 2011a]. We showed in section 4.4 that the same conclusions are reached from consideration of non-log-transformed CHL. While this eddy stirring is dominant in global composites, the results presented here reveal that rich variability exists regionally in the response of CHL. This diversity is averaged out in global composites.

Eddies formed in the major boundary current systems examined here (GS, BMC, EAC, and CCS) entrain and trap elevated CHL into the interiors of cyclones and suppressed CHL into anticyclones during formation. This finding is supported here by maps of $\partial\overline{CHL}/\partial n$, composite averages constructed from hundreds to thousands of weekly observations of CHL'' collocated to the interiors of the eddies identified and tracked in maps of SSH, and in the time evolution of CHL'' within eddies. Time series of CHL'' in the interiors of cyclones in the GS and BMC display statistically significant positive trends, defined as significant changes in CHL'' during the first 12 weeks of the eddies' lifetimes. These trends suggest a CHL response to vertical velocities generated during the intensification of cyclones. Thus, trapping of CHL is common to all the boundary current systems investigated here, whereas CHL enhancement due to eddy intensification is only detectable in two of the four systems. Similarity in CHL responses to eddies in these systems is noteworthy, particularly in light of the differences in physical dynamics among these regimes.

In the interior SIO, eddies contain CHL'' attributable to both the trapping of CHL during eddy formation and a phytoplankton response to W_E, both of which generate positive and negative CHL'' in anticyclones and cyclones, respectively. The collocation of maximum CHL'' with maximum W_E of the same sign, and the increase in CHL'' following eddy formation observed in anticyclones of the interior SIO during the Austral winter suggest that W_E can sustain and enhance the positive CHL'' that is trapped during eddy formation.

The ability to attribute CHL responses in eddies to specific mechanisms is important because the impact on primary production and the export of carbon from the euphotic zone to the ocean interior depends on how the observed CHL'' is generated within eddies. For example, eddy trapping results in the advection of CHL and nutrients from one region to another. On the other hand, the upwelling of nutrients into the euphotic zone within eddies can generate new primary production, possibly enhancing the export of carbon from

the sunlit near-surface to depth. It is important note, however, that anomalies of CHL are not always correlated with changes in phytoplankton biomass. If CHL anomalies are entirely physiological and do not reflect changes in biomass, and particularly if these changes are light driven, then their implications on primary and export production can be quite different [*Behrenfeld et al.*, 2005, 2008; *Siegel et al.*, 2013, 2014].

Although evidence for eddy-driven biophysical processes is observed in each of the regions investigated in section 5, attribution of the observed response in CHL'' to any specific mechanism is ambiguous in most instances. This is because multiple mechanisms produce perturbations in CHL'' of the same sign (Figure 2 and Table 1). In some cases, the temporal evolution of eddy-centric CHL'' can help distinguish mechanisms (Figure 3), however, the trends observed in the CHL'' time series were only marginally statistically significant. In addition, in the interior SIO, seasonal variations that influence the imprint of the eddy-driven processes on near-surface CHL were also observed, further complicating the attribution of observed CHL variability to the specific mechanisms investigated here.

In the future, we plan to investigate other regions where r'_0 is significant. For example, to the north and south of the Hawaiian Islands in the North Pacific, r'_0 and r'_E are both significantly positive (Figures 1a and 1d) and $\partial \overline{CHL}/\partial n$ is negative (Figure 5b). Given that the effects of eddy-induced Ekman pumping and the trapping of CHL during eddy formation are of the same sign, both processes presumably contribute to the observed positive r'_0. There are also open ocean regions where the effects of different mesoscale physical/ biological mechanisms are of opposite sign. For example, the central South Pacific Ocean contains a large region of significantly positive r'_0 and r'_E (Figures 1a and 1d), suggesting that eddy-induced Ekman pumping influences CHL in eddies. Much of this region, however, is associated with negative $\partial \overline{CHL}/\partial n$ (Figure 5b), indicating that during eddy formation, elevated CHL is trapped in cyclones and suppressed CHL is trapped in anticyclones, which is expected to yield negative r'_0. On face value, eddy-induced Ekman pumping thus appears to overshadow trapping in determining the sign of r'_0. However, detailed assessment of the relative importance of the mechanisms awaits further study.

An important limitation of the results presented here is that satellites only observe near-surface CHL. Sometimes large CHL anomalies occur in eddies below the depth observable by satellites [e.g., *Siegel et al.*, 1999; *McGillicuddy et al.*, 2007]. The mechanisms controlling the response of phytoplankton to eddies globally therefore cannot be fully elucidated from satellite observations alone. Further studies, including in situ observations in combination with satellite data and coupled biophysical numerical simulations are needed in order to definitively address the various mechanisms regulating the CHL responses to eddies. The synthesis of the responses of CHL to eddies presented in this study provides a framework that can be utilized to test the ability of coupled biophysical ocean models to reproduce the observed variability.

References

Abraham, E. R. (1998), The generation of plankton patchiness by turbulent stirring, *Nature*, *391*(6667), 577–580.

Andrews, J. C., and P. Scully-Power (1976), The structure of an East Australian Current anticyclonic eddy, *J. Phys. Oceanogr.*, *6*(5), 756–765.

Backus, R., P. Richardson, P. Wiebe, G. Flierl, D. Kester, D. Olson, A. Vastano, and J. Wormuth (1981), Gulf Stream cold-core rings: Their physics, chemistry, and biology, *Science*, *212*, 1091–1100.

Behrenfeld, M., E. Boss, D. Siegel, and D. Shea (2005), Carbon-based ocean productivity and phytoplankton physiology from space, *Global Biogeochem. Cycles*, *19*, GB1006, 1–14, doi:10.1029/2004GB002299.

Behrenfeld, M., K. Halsey, and A. Milligan (2008), Evolved physiological responses of phytoplankton to their integrated growth environment, *Philos. Trans. R. Soc. B*, *363*(1504), 2687–2703.

Behrenfeld, M. J., and P. G. Falkowski (1997), Photosynthetic rates derived from satellite-based chlorophyll concentration, *Limnol. Oceanogr.*, *42*(1), 1–20.

Benitez-Nelson, C. R., et al. (2007), Mesoscale eddies drive increased silica export in the subtropical Pacific Ocean, *Science*, *316*(5827), 1017–1021.

Campbell, J. (1995), The lognormal distribution as a model for bio-optical variability in the sea, *J. Geophys. Res.*, *100*, 13–13.

Chaigneau, A., G. Eldin, and B. Dewitte (2009), Eddy activity in the four major upwelling systems from satellite altimetry (1992–2007), *Prog. Oceanogr.*, *83*(1), 117–123.

Chelton, D., and M. Freilich (2005), Scatterometer-based assessment of 10-m wind analyses from the operational ECMWF and NCEP numerical weather prediction models, *Mon. Weather Rev.*, *133*(2), 409–429.

Chelton, D., and S. Xie (2010), Coupled ocean-atmosphere interaction at oceanic mesoscales, *Oceanography*, *23*, 52–69.

Chelton, D., M. Schlax, M. Freilich, and R. Milliff (2004), Satellite measurements reveal persistent small-scale features in ocean winds, *Science*, *303*(5660), 978–983.

Chelton, D., P. Gaube, M. Schlax, J. Early, and R. Samelson (2011a), The influence of nonlinear mesoscale eddies on near-surface oceanic chlorophyll, *Science*, *334*(6054), 328–332.

Chelton, D., M. Schlax, and R. Samelson (2011b), Global observations of nonlinear mesoscale eddies, *Progr. Oceanogr.*, *91*(2), 167–216.

Cullen, J. J. (1982), The deep chlorophyll maximum: Comparing vertical profiles of chlorophyll a, *Can. J. Fish. Aquat. Sci.*, *39*(5), 791–803.

Dewar, W., and G. Flierl (1987), Some effects of the wind on rings, *J. Phys. Oceanogr.*, *17*(10), 1653–1667.

d'Ovidio, F., S. De Monte, A. Della Penna, C. Cotté, and C. Guinet (2013), Ecological implications of eddy retention in the open ocean: A Lagrangian approach, *J. Phys. A Math. Theor., 46*(25), 254,023.

Ducet, N., P.-Y. Le Traon, and G. Reverdin (2000), Global high-resolution mapping of ocean circulation from TOPEX/Poseidon and ERS-1 and-2, *J. Geophys. Res., 105*(C8), 19,477–19,498.

Early, J., R. Samelson, and D. Chelton (2011), The evolution and propagation of quasigeostrophic ocean eddies, *J. Phys. Oceanogr., 41*(8), 1535–1555.

Ebbesmeyer, C. C., and E. J. Lindstrom (1986), Structure and origin of 18°C water observed during the POLYMODE local dynamics experiment, *J. Phys. Oceanogr., 16*(3), 443–453.

Fairall, C., E. Bradley, J. Hare, A. Grachev, and J. Edson (2003), Bulk parameterization of air-sea fluxes: Updates and verification for the COARE algorithm, *J. Clim., 16*(4), 571–591.

Falkowski, P., and J. LaRoche (1991), Acclimation to spectral irradiance in algae, *J. Phycol., 27*(1), 8–14.

Falkowski, P., D. Ziemann, Z. Kolber, and P. Bienfang (1991), Role of eddy pumping in enhancing primary production in the ocean, *Nature, 352*(6330), 55–58.

Feng, M., L. J. Majewski, C. B. Fandry, and A. M. Waite (2007), Characteristics of two counter-rotating eddies in the Leeuwin Current system off the Western Australian Coast, *Deep Sea Res., Part II, 54*, 961–980.

Flierl, G., and D. McGillicuddy (2002), Mesoscale and submesoscale physical-biological interactions, in *Biological-Physical Interactions in the Sea, Sea: Ideas Obs. Prog. Study Seas Ser.,* vol. 12, edited by A. R. Robinson, J. J. McCarthy, and B. J. Rothschild, pp. 113–185, John Wiley, N. Y.

Flierl, G. R. (1981), Particle motions in large-amplitude wave fields, *Geophys. Astrophys. Fluid Dyn., 18*(1–2), 39–74.

Franks, P., J. Wroblewski, and G. Flierl (1986), Prediction of phytoplankton growth in response to the frictional decay of a warm-core ring, *J. Geophys. Res., 91*(C6), 7603–7610.

Fu, L.-L., and R. Ferrari (2008), Observing oceanic submesoscale processes from space, *Eos Trans. AGU, 89*(48), 488–488.

Garver, S. A., and D. Siegel (1997), Inherent optical property inversion of ocean color spectra and its biogeochemical interpretation: I. Time series from the Sargasso Sea, *J. Geophys. Res., 102*, 18,607–18,625.

Gaube, P. (2012), Satellite observations of the influence of mesoscale ocean eddies on near-surface temperature, phytoplankton and surface stress, PhD thesis, Oreg. State Univ., Corvallis.

Gaube, P., D. Chelton, P. Strutton, and M. Behrenfeld (2013), Satellite observations of chlorophyll, phytoplankton biomass and Ekman pumping in nonlinear mesoscale eddies, *J. Geophys. Res. Oceans, 118*, 6349–6370, doi:10.1002/2013JC009027.

Gaube, P., D. B. Chelton, R. M. Samelson, M. G. Schlax, and L. W. O'Neill (2014a), Satellite Observations of Mesoscale Eddy-Induced Ekman Pumping, *J. Phys. Oceanogr.*, doi:10.1175/JPO-D-14-0032.1, in press.

Geider, R. (1987), Light and temperature dependence of the carbon to chlorophyll a ratio in microalgae and cyanobacteria: Implications for physiology and growth of phytoplankton, *New Phytol., 106*(1), 1–34.

Laws, E., and T. Bannister (1980), Nutrient-and light-limited growth of *Thalassiosira fluviatilis* in continuous culture, with implications for phytoplankton growth in the ocean, *Limnol. Oceanogr., 25*(3), 457–473.

Ledwell, J., D. McGillicuddy Jr., and L. Anderson (2008), Nutrient flux into an intense deep chlorophyll layer in a mode-water eddy, *Deep Sea Res., Part II, 55*(10–13), 1139–1160.

Legal, C., P. Klein, A.-M. Treguier, and J. Paillet (2007), Diagnosis of the vertical motions in a mesoscale stirring region, *J. Phys. Oceanogr., 37*(5), 1413–1424.

Lehahn, Y., F. d'Ovidio, M. Lévy, Y. Amitai, and E. Heifetz (2011), Long range transport of a quasi isolated chlorophyll patch by an Agulhas ring, *Geophys. Res. Lett., 38*, L16610, doi:10.1029/2011GL048588.

Lévy, M., L. Mémery, and G. Madec (1998), The onset of a bloom after deep winter convection in the northwestern Mediterranean sea: Mesoscale process study with a primitive equation model, *J. Mar. Syst., 16*(1), 7–21.

Lévy, M., L. Mémery, and G. Madec (1999), The onset of the spring bloom in the MEDOC area: Mesoscale spatial variability, *Deep Sea Res., Part I, 46*(7), 1137–1160.

Lévy, M., R. Ferrari, P. Franks, A. Martin, and P. Rivière (2012), Bringing physics to life at the submesoscale, *Geophys. Res. Lett., 39*, L14602, doi:10.1029/2012GL052756.

Mahadevan, A., N. Thomas, L, and A. Tandon (2008), Comments on "Eddy/wind interactions stimulate extraordinary mid-ocean plankton blooms," *Science, 320*, 448.

Maritorena, S., D. Siegel, and R. Peterson (2002), Optimization of a semianalytical ocean color model for global-scale applications, *Appl. Opt., 41*(15), 2705–2714.

Martin, A., and K. Richards (2001), Mechanisms for vertical nutrient transport within a North Atlantic mesoscale eddy, *Deep Sea Res., Part II, 48*(4–5), 757–773.

McGillicuddy, D., A. Robinson, D. Siegel, H. Jannasch, R. Johnson, T. Dickey, J. McNeil, A. Michaels, and A. Knap (1998), Influence of mesoscale eddies on new production in the Sargasso Sea, *Nature, 394*(6690), 263–266.

McGillicuddy, D. J., et al. (1999), Mesoscale variations of biogeochemical properties in the Sargasso Sea. *J. Geophys. Res. Oceans, 104*(C6), 13381–13394.

McGillicuddy, D., et al. (2007), Eddy/wind interactions stimulate extraordinary mid-ocean plankton blooms, *Science, 316*(5827), 1021.

McGillicuddy, D., J. Ledwell, and L. Anderson (2008), Response to comments on "Eddy/Wind interactions stimulate extraordinary mid-ocean plankton bloom," *Science, 320*, 488.

McWilliams, J., and G. Flierl (1979), On the evolution of isolated, nonlinear vortices, *J. Phys. Oceanogr., 9*(6), 1155–1182.

Moore, T., R. Matear, J. Marra, and L. Clementson (2007), Phytoplankton variability off the Western Australian Coast: Mesoscale eddies and their role in cross-shelf exchange, *Deep Sea Res., Part II, 54*(8–10), 943–960.

Olson, D. B. (1986), Lateral exchange within Gulf Stream warm-core ring surface layers, *Deep Sea Res., Part A, 33*(11), 1691–1704.

O'Neill, L., D. Chelton, and S. Esbensen (2010), The effects of SST-induced surface wind speed and direction gradients on midlatitude surface vorticity and divergence, *J. Clim., 23*(2), 255–281.

Pearce, A., and R. Griffiths (1991), The mesoscale structure of the Leeuwin Current: A comparison of laboratory models and satellite imagery, *J. Geophys. Res., 96*(C9), 16,739–16,757.

Rio, M., S. Guinehut, and G. Larnicol (2011), New CNES-CLS09 global mean dynamic topography computed from the combination of GRACE data, altimetry, and in situ measurements, *J. Geophys. Res., 116*, C07018, doi:10.1029/2010JC006505.

Ross, D., J. Overland, W. Plerson, V. Cardone, R. McPherson, and T. Yu (1985), Oceanic surface winds, *Adv. Geophys., 27*, 101–140.

Samelson, R., M. Schlax, and D. Chelton (2013), Randomness, symmetry and scaling of mesoscale eddy life cycles, *J. Phys. Oceanogr., 44*, 1012–1029.

Siegel, D., D. McGillicuddy, and E. Fields (1999), Mesoscale eddies, satellite altimetry, and new production in the Sargasso Sea, *J. Geophys. Res.*, *104*(C6), 13,359–13,380.

Siegel, D., S. Maritorena, N. Nelson, D. Hansell, and M. Lorenzi-Kayser (2002), Global distribution and dynamics of colored dissolved and detrital organic materials, *J. Geophys. Res.*, *107*(C12), 3228.

Siegel, D., D. Court, D. Menzies, P. Peterson, S. Maritoena, and N. Nelson (2007), Satellite and in situ observation of the bio-optical signatures of two mesoscale eddies in the Sargasso Sea, *Deep Sea Res., Part II*, *55*, 1218–1230.

Siegel, D., P. Peterson, D. McGillicuddy Jr., S. Maritorena, and N. Nelson (2011), Bio-optical footprints created by mesoscale eddies in the Sargasso Sea, *Geophys. Res. Lett.*, *38*, L13608, doi:10.1029/2011GL047660.

Siegel, D., et al. (2013), Regional to global assessments of phytoplankton dynamics from the SeaWiFS mission, *Remote Sens. Environ.*, *135*, 77–91.

Siegel, D. A., K. O. Buesseler, S. C. Doney, S. F. Sailley, M. J. Behrenfeld, and P. W. Boyd (2014), Global assessment of ocean carbon export by combining satellite observations and food-web models, *Global Biogeochem. Cycles*, *28*(3), 181–196.

Small, R., S. DeSzoeke, S. Xie, L. O'Neill, H. Seo, Q. Song, P. Cornillon, M. Spall, and S. Minobe (2008), Air-sea interaction over ocean fronts and eddies, *Dyn. Atmos. Oceans*, *45*(3–4), 274–319.

Sweeney, E. N., D. J. McGillicuddy Jr., and K. O. Buesseler (2003), Biogeochemical impacts due to mesoscale eddy activity in the Sargasso Sea as measured at the Bermuda Atlantic Time-series Study (BATS), *Deep Sea Res., Part II*, *50*(22), 3017–3039.

Thomas, L. N. (2005), Destruction of potential vorticity by winds, *J. Phys. Oceanogr.*, *35*(12), 2457–2466.

Thomas, L. N., and P. B. Rhines (2002), Nonlinear stratified spin-up, *J. Fluid Mech.*, *473*, 211–244.

Von Storch, H., and F. Zwiers (1999), *Statistical Analysis in Climate Research*, Cambridge Univ. Press, Cambridge, U. K.

Waite, A., S. Pesant, D. Griffin, P. Thompson, and C. Holl (2007a), Oceanography, primary production and dissolved inorganic nitrogen uptake in two Leeuwin Current eddies, *Deep Sea Res., Part II*, *54*(8–10), 981–1002.

Waite, A., et al. (2007b), The Leeuwin Current and its eddies: An introductory overview, *Deep Sea Res., Part II*, *54*(8–10), 789–796.

Wiebe, P., and G. Flierl (1983), Euphausiid invasion/dispersal in Gulf Stream cold-core rings, *Mar. Freshwater Res.*, *34*(4), 625–652.

Wiebe, P., E. Hulburt, E. Carpenter, A. E. Jahn, G. Knapp, S. Boyd, P. Ortner, and J. Cox (1976), Gulf Stream cold-core rings: Large-scale interaction sites for open ocean plankton communities, *Deep Sea Res. Oceanogr. Abstr.*, *23*, 695–710.